Research Square

Preprints are preliminary reports that have not undergone peer review.
They should not be considered conclusive, used to inform clinical practice,
or referenced by the media as validated information.

Thermal Conversion Pathways of Chontaduro (Bactris gasipaes Kunth) Rachis: Kinetic, Evolved-Gas, and Operational Assessment for Carbon-Enriched Products

Oscar Danilo Guerra Ceballos
Universidad Nacional de Colombia
Wilson Daniel Caicedo Chacon
w.caicedo.ch@gmail.com

Fundación Universitaria Agraria de Colombia

Research Article

Keywords: Chontaduro rachis, agro-industrial residue, thermochemical conversion, biomass biorefinery, evolved gas analysis, isoconversional kinetics

Posted Date: November 6th, 2026

DOI: https://doi.org/10.21203/rs.3.rs-10259836/v1

License: This work is licensed under a Creative Commons Attribution 4.0 International License.
Read Full License

Additional Declarations: No competing interests reported.

Thermal Conversion Pathways of Chontaduro (Bactris gasipaes Kunth) Rachis: Kinetic, Evolved-Gas, and Operational Assessment for Carbon-Enriched Products

Oscar Danilo Guerra Ceballos[a], Wilson Daniel Caicedo Chacon[b,*]

[a]Facultad de Ingeniería y Administración, Universidad Nacional de Colombia sede Palmira, Colombia AA 237, Palmira, Colombia

[b]Ingeniería de Alimentos, Fundación Universitaria Agraria de Colombia, Calle 170 #54a-10, CP 111156 Bogotá, Colombia

Guerra D.F.G.: ORCID: 0009-0000-6414-9574, email: odguerrac@unal.edu.co

Chacon W.D.C.: ORCID: 0000-0002-8391-4849, email: w.caicedo.ch@gmail.com

[*] Corresponding author: PhD. Wilson Daniel Caicedo Chacon, Ingeniería de Alimentos, Fundación Universitaria Agraria de Colombia, Calle 170 #54a-10, CP 111156 Bogotá, Colombia. E-mail address: w.caicedo.ch@gmail.com (W.D.C. Chacon).

Abstract

Chontaduro (*Bactris gasipaes* Kunth) rachis is an underutilized agro-industrial residue with potential as a lignocellulosic feedstock for thermochemical conversion and biorefinery applications. This study investigated its thermal conversion behavior by integrating multi-rate thermogravimetric and derivative thermogravimetric analysis (TGA/DTG), differential scanning calorimetry (DSC), evolved-gas mass spectrometry (EGA-MS), and isoconversional kinetic modeling. Thermal decomposition proceeded through three main regimes: dehydration between 25 and 150 °C, active devolatilization from approximately 162 to 277 °C, and progressive carbonization up to 700 °C. The active devolatilization stage accounted for nearly 35–37% mass loss and was associated with the synchronized evolution of CO_2, H_2O, and NH_3-related fragments near the principal DTG maximum. Flynn–Wall–Ozawa and Friedman analyses revealed conversion-dependent activation energies, indicating a transition from labile carbohydrate-rich structures to more recalcitrant cellulose- and lignin-derived domains. Differential master plots identified an Avrami–Erofeev-type behavior as the best apparent descriptor of the devolatilization stage, while thermal-shift factors confirmed that heating rate effects were conversion-dependent rather than uniform. The conversion–temperature map further enabled the identification of mild, torrefaction-like, and advanced carbonization windows for producing partially devolatilized or carbon-enriched solid products. Overall, this work provides a biorefinery-oriented framework linking feedstock composition, volatile evolution, kinetic barriers, and operational thermal-severity selection for the valorization of chontaduro rachis.

Keywords: Chontaduro rachis; agro-industrial residue; thermochemical conversion; biomass biorefinery; evolved gas analysis; isoconversional kinetics

1. Introduction

The valorization of agro-industrial residues has become a strategic pathway within the circular bioeconomy, particularly because lignocellulosic by-products can be converted into bioenergy carriers, platform chemicals, functional fractions, bio-based materials, and carbon-rich solids through integrated biorefinery approaches. Agricultural and agro-food residues are generated in large quantities worldwide and are increasingly regarded not as waste streams but as renewable feedstocks for value-added conversion routes. In this context, lignocellulosic biomass is especially relevant because its cellulose, hemicellulose, lignin, extractives, proteins, and mineral fractions can define multiple thermochemical, biochemical, and physicochemical valorization pathways. Chontaduro or peach palm (*Bactris gasipaes* Kunth) is an underutilized tropical palm with important food and agro-industrial relevance in Latin America, and previous studies have highlighted the potential of its processing by-products as sources of dietary fiber, bioactive compounds, enzymes, fermentable sugars, xylooligosaccharides, and other value-added products. However, the rachis, which constitutes the lignocellulosic axis supporting the infructescence, remains scarcely explored as a thermochemical conversion feedstock despite its fibrous structure and potential suitability for torrefaction, carbonization, and bio-based solid product development. Therefore, understanding its thermal stability, devolatilization behavior, and conversion-dependent reactivity is essential for assessing its feasibility within biomass biorefinery and circular-economy schemes [1, 2, 3, 4, 5].

Thermochemical conversion of lignocellulosic biomass is governed by a complex sequence of overlapping reactions rather than by a single degradation event. During non-isothermal heating, biomass typically undergoes moisture removal, depolymerization of labile hemicellulosic and amorphous carbohydrate domains, cellulose-rich devolatilization, lignin fragmentation, secondary cracking, condensation, aromatization, and progressive char formation. These transformations depend strongly on feedstock composition, particle properties, heating rate, thermal history, and inorganic matter, which may alter both degradation pathways and product distribution. Thermogravimetric analysis and derivative thermogravimetry provide a direct means to quantify mass-loss dynamics, onset and peak temperatures, devolatilization intensity, and residual char yield, whereas differential scanning calorimetry complements these data by identifying endothermic and exothermic transitions associated with water release, structural relaxation, bond cleavage, condensation, and carbonization reactions. The combined use of TGA/DTG and DSC is therefore particularly useful for distinguishing physical events from chemically driven transformations and for linking thermal conversion stages with the energetic response of the biomass matrix [6, 7, 8].

Although TGA/DTG and DSC provide essential thermal and kinetic descriptors, conventional thermoanalytical profiles are often chemically ambiguous when applied to heterogeneous biomass. DTG peaks are frequently assigned to hemicellulose, cellulose, lignin, proteins, extractives, or starch-like fractions based mainly on temperature ranges, but such assignments may remain tentative if they are not supported by direct volatile-evolution evidence. Hyphenated evolved-gas analysis techniques, including TGA-MS, TGA-FTIR, and TGA-GC-MS, help overcome this limitation by detecting gaseous and volatile fragments released during thermal conversion. In particular, evolved-gas mass spectrometry enables the temperature-resolved monitoring of diagnostic ions associated with H_2O, CO_2, CO, NH_3-related fragments, hydrocarbons, oxygenated species, and nitrogen-containing compounds. This information allows mass-loss events to be correlated with probable dehydration, decarboxylation, deamination, depolymerization, cracking, and char-reorganization pathways. For biomass pyrolysis and carbonization studies, such coupling is valuable because it connects macroscopic thermal events with molecular-level volatile signatures and improves the mechanistic interpretation of conversion stages [9, 10, 11].

From a kinetic perspective, non-isothermal biomass conversion is commonly evaluated through global and isoconversional approaches. The Kissinger method remains widely used because it estimates an apparent activation energy from the displacement of peak temperatures with heating rate; however, it provides a single global value and may mask the complexity of multi-step processes. For heterogeneous biomass, this limitation is especially important because the apparent activation energy can vary substantially with conversion as different pseudo-components dominate the reaction pathway. Isoconversional methods such as Flynn–Wall–Ozawa and Friedman enable the estimation of conversion-dependent activation energies without imposing a fixed reaction model, making them more suitable for identifying changes in kinetic barriers during progressive devolatilization and carbonization. Recent ICTAC recommendations emphasize that reliable interpretation of thermal decomposition kinetics requires careful selection of conversion intervals, multiple heating rates, evaluation of model assumptions, and avoidance of overinterpreting linear fits as evidence of single-step mechanisms [12, 13, 14, 15, 16].

For biomass conversion and biorefinery applications, kinetic descriptors are most useful when they are linked to operational severity and product-oriented thermal windows. In this sense, conversion-

normalized approaches, master-plot comparisons, and thermal-shift analysis can help determine whether heating-rate effects represent a simple temperature displacement or reflect conversion-dependent changes in the apparent reaction network. Such information is relevant for selecting mild pretreatment, torrefaction-like, or advanced carbonization conditions aimed at tailoring solid yield, volatile removal, fixed-carbon enrichment, ash concentration, and potential fuel or material properties. Because lignocellulosic materials commonly exhibit overlapping pseudo-component degradation, the apparent reaction model obtained from master plots should be interpreted as a macroscopic descriptor of the dominant conversion behavior rather than as proof of a unique molecular mechanism. Integrating TGA/DTG, DSC, EGA-MS, isoconversional kinetics, and operational conversion mapping can therefore provide a stronger basis for translating laboratory thermoanalysis into biomass conversion and biorefinery decision-making [15, 16, 8, 6].

Despite growing interest in the valorization of *Bactris gasipaes* residues, most available studies have focused on food, nutritional, enzymatic, composting, saccharification, or biochemical uses, whereas the thermochemical conversion behavior of chontaduro rachis remains poorly understood. In particular, there is still limited information on how its composition controls devolatilization, evolved-gas formation, conversion-dependent activation energy, and the transition from carbohydrate-rich decomposition to carbon-enriched solid formation. This knowledge gap restricts the rational selection of thermal-processing conditions for its use as a biorefinery feedstock. We hypothesize that chontaduro rachis powder undergoes composition-controlled, multi-step thermal conversion in which specific volatile emissions co-localize with major DTG events and conversion-dependent kinetic barriers, reflecting a progressive transition from labile polysaccharide degradation to lignin-derived aromatization and char evolution. Addressing this hypothesis requires an integrated framework capable of linking feedstock composition, thermal events, volatile fingerprints, kinetic parameters, and operational conversion targets [2, 4, 5, 10].

Therefore, the objective of this study was to develop an integrated thermo-kinetic and evolved-gas framework to describe the thermal conversion pathways of chontaduro (*Bactris gasipaes* Kunth) rachis as an agro-industrial lignocellulosic residue for biorefinery-oriented valorization. For this purpose, multi-rate thermogravimetric and derivative thermogravimetric analysis, differential scanning calorimetry, evolved-gas mass spectrometry, Kissinger, Flynn–Wall–Ozawa, and Friedman kinetic methods, differential master plots, thermal-shift analysis, and statistical validation tools were combined. By coupling mass-loss behavior, enthalpic transitions, volatile-emission profiles, conversion-dependent activation energies, and operational conversion–temperature mapping, this work aims to establish a mechanistic basis for selecting thermal-treatment windows associated with mild devolatilization, torrefaction-like transformation, and advanced carbonization. The resulting approach is intended to support the conversion of chontaduro rachis from an underused agro-industrial residue into a potential feedstock for carbon-enriched solids and other non-food biorefinery products [16, 9, 6, 3].

2. Materials and Methods

2.1 Raw material (biomatrix) and preparation

Fresh chontaduro (*Bactris gasipaes* Kunth) rachis was collected as an agro-industrial by-product generated during fruit cluster processing. The selected material corresponded to the main lignocellulosic axis of the infructescence, as schematically shown in **Fig. 1A–B**. Peach palm processing residues have been reported as lignocellulosic by-products with potential for valorization into prebiotics, enzymes, cellulose-based materials, high-fiber fractions, and other bio-based products [2, 5]. Therefore, **Fig. 1** is included to contextualize the anatomical origin of the rachis and to illustrate its expected cellulose-, hemicellulose-, lignin-, extractive-, and ash-containing organization as a biomass matrix. The compositional scheme should be interpreted as a conceptual representation unless the structural fractions were independently quantified in this study.

The rachis was washed with distilled water to remove adhering impurities, cut into 1–2 cm fragments, and convectively dried at 60 ± 2 °C until constant mass. Drying was performed to reduce moisture content, improve sample stability, and facilitate subsequent milling and sieving, in accordance with common biomass preparation practices for compositional and thermoanalytical studies [17, 18]. The dried material was milled and sieved to obtain a particle-size fraction of 250–500 µm. This controlled fraction was selected to improve sample homogeneity and reduce heat- and mass-transfer limitations during thermogravimetric measurements, since particle size can affect volatile diffusion, internal thermal gradients, secondary charring, and apparent kinetic behavior during biomass pyrolysis and thermal analysis [19, 20, 21].

The resulting powder was stored in airtight containers over silica gel desiccant at ambient temperature to minimize moisture re-adsorption prior to proximate, thermogravimetric, calorimetric, and evolved-gas analyses. This standardized preparation protocol was intended to improve analytical repeatability and support reliable comparison of thermal conversion behavior across heating rates.

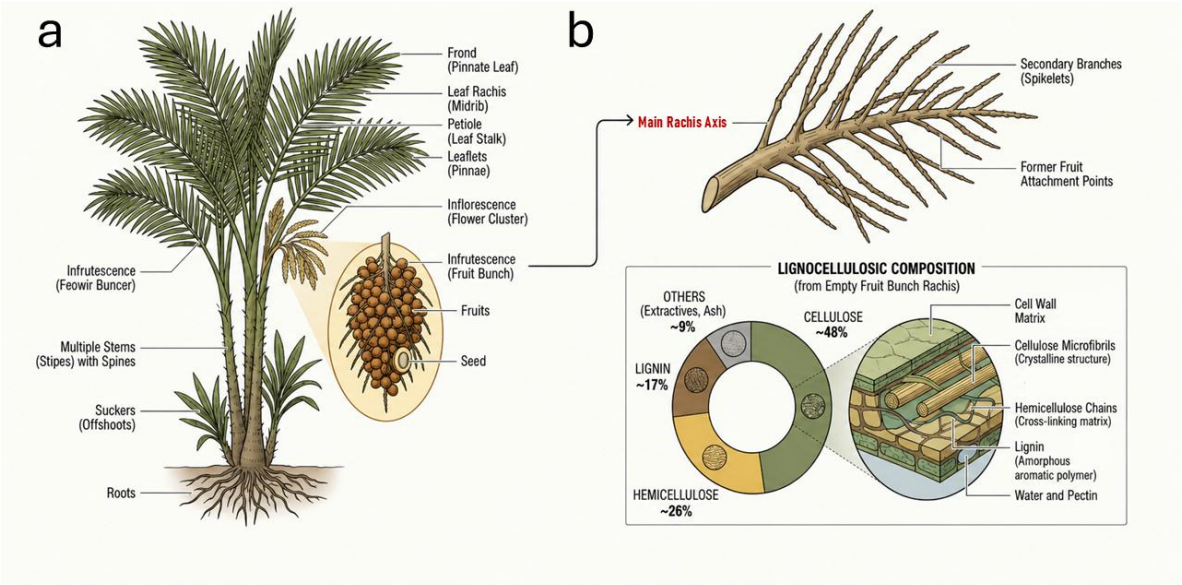


Fig 1 Morphological and macromolecular representation of *Bactris gasipaes*: (a) General botanical structure of the chontaduro palm with explicit localization of the rachis; (b) Schematic magnification of the fiber-rich biomatrix showing its primary lignocellulosic components (cellulose, hemicellulose, and lignin)

2.2 Proximal composition analysis

The proximate composition of Bactris gasipaes Kunth rachis powder was determined to establish a compositional basis for interpreting its thermoanalytical and evolved-gas behavior. Moisture, ash, crude protein, crude lipid, total dietary fiber, and carbohydrate contents were quantified using standardized analytical procedures commonly applied to food, agricultural, and plant-derived matrices [22, 23]. Proximate composition was subsequently used to support the interpretation of dehydration, devolatilization intensity, mineral residue formation, nitrogen-containing volatile evolution, and residual char generation during thermal conversion, as biomass composition has been shown to influence thermogravimetric profiles, ash formation, combustion/pyrolysis behavior, and kinetic descriptors [24, 21].

Moisture content was determined gravimetrically by oven drying the samples at 105 °C until constant weight, while ash content was quantified by calcination in a muffle furnace at 550 °C. Crude protein was estimated from total nitrogen determined by the Kjeldahl method using a nitrogen-to-protein conversion factor of 6.25, and crude lipid content was measured by Soxhlet extraction using petroleum ether as solvent, following conventional proximate analysis procedures [22]. Total dietary fiber was quantified using an enzymatic–gravimetric procedure, in which digestible starch and protein are enzymatically removed and the remaining residue is corrected for residual ash and protein [23]. Carbohydrate content was calculated by difference according to Eq. 1.

$$\%Carbohydrates = 100 - (\%Moisture + \%Protein + \%Lipids + \%Ash + \%Fiber) \quad \textbf{(1)}$$

All analyses were performed in triplicate, and results were expressed as mean ± standard deviation on a wet basis (% w/w). The resulting compositional profile was integrated with TGA/DTG, DSC, and EGA-MS data to support the interpretation of thermal degradation stages, devolatilization behavior, evolved-gas formation, and residual char development during thermochemical conversion of the rachis biomass.

2.3 Thermogravimetric analysis (TGA/DTG)

2.3.1 Experimental design

Dynamic thermogravimetric analyses were performed under non-isothermal conditions at four linear heating rates: β = 5, 10, 15, and 20 °C min^{-1}, over the temperature range of 25–700 °C. The thermogravimetric response was continuously recorded as residual mass (%) and derivative thermogravimetric signal (DTG, % °C^{-1}) as a function of temperature. The use of multiple heating

rates was selected to evaluate peak displacement, thermal-lag effects, conversion-dependent behavior, and kinetic consistency during the main devolatilization stage. Multi-rate non-isothermal experiments are widely recommended for kinetic analysis of thermally stimulated solid-state processes, particularly when biomass degradation involves overlapping reactions and apparent multi-step behavior [16, 8].

Detailed point-by-point TGA/DTG datasets for the four heating rates, including temperature, residual mass, and DTG signal, are provided as **Online Resource 1** to allow independent reconstruction of the thermal profiles.

The linear heating rate was defined according to Eq. 2:

$$\beta = \frac{dT}{dt} \tag{2}$$

where β is the heating rate, T is temperature, and t is time.

2.3.2 Thermal stage identification and characteristic temperatures

Thermal decomposition stages were identified from the TGA and DTG profiles by considering the main mass-loss regions and their corresponding derivative events. Three thermal regions were considered: (i) dehydration between 25 and 150 °C, mainly associated with moisture release and weakly bound water removal; (ii) active devolatilization between approximately 162 and 277 °C, corresponding to the dominant mass-loss event of the lignocellulosic matrix; and (iii) progressive carbonization and secondary cracking above 300 °C. Similar multi-stage thermal behavior has been widely reported for lignocellulosic biomass and is commonly attributed to the superposition of hemicellulose, cellulose, lignin, extractives, inorganic matter, and secondary char-forming reactions [25, 6, 8].

For the active devolatilization stage, the onset temperature ($T_{on,2}$) was defined as the beginning of the main DTG event, the maximum degradation temperature ($T_{max,2}$) as the temperature of the dominant DTG peak, and the endset temperature ($T_{end,2}$) as the minimum or inflection region separating the main devolatilization event from the subsequent high-temperature degradation domain. For the present dataset, the adopted $T_{on,2}$ values were 163.501, 163.413, 161.889, and 164.017 °C, while the corresponding $T_{end,2}$ values were 264.429, 271.192, 273.898, and 276.603 °C for 5, 10, 15, and 20 °C min^{-1}, respectively. The use of DTG-derived descriptors is appropriate for identifying peak displacement, maximum degradation rate, and stage boundaries in biomass thermal conversion studies [25, 6].

The thermal conversion degree was calculated according to Eq. 3:

$$\alpha(T) = \frac{m_0 - m(T)}{m_0 - m_f} \tag{3}$$

where m_0 is the initial mass at 25 °C, $m(T)$ is the instantaneous mass at temperature T, and m_f is the final residual mass at 700 °C.

Under linear heating conditions, the decomposition rate was expressed according to Eq. (4).

$$\frac{d\alpha}{dt} = \beta \frac{d\alpha}{dT} \tag{4}$$

The general solid-state kinetic equation was expressed as:

$$\frac{d\alpha}{dt} = k(T)\, f(\alpha) \tag{5}$$

where $k(T)$ is the temperature-dependent rate constant and $f(\alpha)$ is the differential reaction model.

The temperature dependence of the kinetic constant followed the Arrhenius relationship described in Eq. (6).

$$k(T) = A \exp\left(-\frac{E_a}{RT}\right) \tag{6}$$

where A is the pre-exponential factor, E_a is the apparent activation energy, R is the universal gas constant, and T is the absolute temperature.

By combining Eqs. (4)–(6), the non-isothermal rate expression becomes Eq. 7:

$$\beta \frac{d\alpha}{dT} = A \exp\left(-\frac{E_a}{RT}\right) f(\alpha) \tag{7}$$

This equation provides the mathematical basis for linking the experimental TGA/DTG data with subsequent isoconversional kinetic treatment and master-plot analysis. The use of conversion-based kinetic expressions is particularly relevant for heterogeneous biomass, where apparent activation energy and reaction mechanism may vary with conversion due to overlapping pseudo-component degradation and secondary char-forming reactions [16, 26].

2.4 Master curves for the active devolatilization stage

2.4.1 Stage-normalized conversion and thermal superposition

Because the global conversion degree, α, includes the initial dehydration region and the high-temperature carbonization domain, a stage-normalized conversion, α_2, was defined specifically for the active devolatilization stage delimited by $T_{on,2}$ and $T_{end,2}$. This normalization was used to isolate the principal devolatilization event and enable direct comparison among heating rates. Such conversion-window selection is recommended for complex solid-state processes in which the global degradation profile involves overlapping reactions and different apparent kinetic regimes [16].

The stage-normalized conversion was calculated according to Eq. 8:

$$\alpha_2(T) = \frac{m(T_{on}) - m(T)}{m(T_{on}) - m(T_{end})} \quad (8)$$

where $m(T_{on})$ and $m(T_{end})$ correspond to the sample masses at the onset and endset temperatures of the devolatilization stage, respectively.

A reference heating rate of 10 °C·min^{-1} was selected for thermal alignment. The temperature-shift factor associated with each conversion coordinate was determined according to Eq. (9).

$$\Delta T(\alpha_2, \beta) = T_\beta(\alpha_2) - T_{\beta_{ref}}(\alpha_2) \quad (9)$$

where $T\beta(\alpha_2)$ is the temperature associated with a given stage-normalized conversion at heating rate β, and $T_{\beta,ref}(\alpha_2)$ is the equivalent temperature at the reference heating rate. Mean thermal shifts were evaluated within α_2 = 0.4–0.9, a region selected to reduce the influence of early-stage baseline uncertainty and terminal-stage noise. For the present dataset, the average shift factors were approximately −7.93, 0.00, 1.29, and 6.55 °C for 5, 10, 15, and 20 °C min^{-1}, respectively. This approach allowed the heating-rate effect to be evaluated as a function of conversion rather than as a single global displacement of the thermal profile. Similar conversion-based approaches are useful when thermal events are affected by pseudo-component overlap, thermal lag, and secondary reactions during biomass conversion [27, 8].

2.4.2 Differential kinetic master plots

In addition to thermal superposition, differential kinetic master plots were used to compare the experimental devolatilization profile with theoretical solid-state reaction models. Master plots provide a normalized way to evaluate whether the experimental conversion-rate profile is compatible with idealized kinetic functions, although their interpretation should be cautious when the process is multi-step or when the apparent activation energy varies significantly with conversion [28, 27].

The experimental reduced-rate function was calculated according to Eq. 10:

$$y_{\exp}(\alpha_2) = \frac{\left(\frac{d\alpha_2}{dT}\right)_{\alpha_2}}{\left(\frac{d\alpha_2}{dT}\right)_{\alpha_2=0.5}} \quad (10)$$

Because each experiment was performed at constant heating rate, the same reduced-rate function can also be expressed in time-derivative form as Eq. 11:

$$y_{\exp}(\alpha_2) = \frac{\left(\frac{d\alpha_2}{dt}\right)_{\alpha_2}}{\left(\frac{d\alpha_2}{dt}\right)_{\alpha_2=0.5}} \quad (11)$$

The corresponding normalized theoretical master curves were expressed according to Eq. 12:

$$y_{\mathrm{th}}(\alpha) = \frac{f(\alpha)}{f(0.5)} \quad (12)$$

where $f(\alpha)$ is the differential reaction model. This normalization at α = 0.5 enables comparison among models with different rate-function magnitudes and focuses the analysis on the shape of the conversion-rate profile [28, 27].

In the present work, the candidate models included reaction-order models (F1, F2, F3), Avrami–Erofeev nucleation models (A2, A3), and contracting-geometry models (R2, R3). These model families are widely used in solid-state kinetic analysis and represent deceleratory reaction-order behavior, nucleation-and-growth-type behavior, and phase-boundary-controlled geometrical contraction, respectively [29]. The theoretical solid-state kinetic models and differential reaction functions used in the master-plot analysis are summarized in **Table 1**.

[Insert Table 1 here]

Table 1. Theoretical solid-state kinetic models and differential reaction functions used in the master-plot analysis of active devolatilization

Model family	**Model**	**Differential reaction function**
Reaction-order model	F1	$\boldsymbol{f(\alpha) = 1 - \alpha}$
Reaction-order model	F2	$\boldsymbol{f(\alpha) = (1 - \alpha)^2}$
Reaction-order model	F3	$\boldsymbol{f(\alpha) = (1 - \alpha)^3}$
Avrami–Erofeev model	A2	$\boldsymbol{f(\alpha) = 2(1 - \alpha)[-ln(1 - \alpha)]^{\frac{1}{2}}}$

Avrami–Erofeev model	A3	$\boldsymbol{f(\alpha) = 3(1-\alpha)[-ln(1-\alpha)]^{\frac{1}{3}}}$
Geometrical contraction model	R2	$\boldsymbol{f(\alpha) = 2(1-\alpha)^{\frac{1}{2}}}$
Geometrical contraction model	R3	$\boldsymbol{f(\alpha) = 3(1-\alpha)^{\frac{2}{3}}}$

The comparison between $y_{exp}(\alpha_2)$ and $y_{th}(\alpha)$ was performed over α_2 = 0.05–0.95 to minimize distortions associated with the initial baseline region and terminal-stage noise. Based on the normalized fitting metrics obtained from the treated dataset, A3 provided the lowest RMSE, followed by A2 and R2. Therefore, the A3-type model was retained as the best apparent descriptor of the normalized devolatilization-rate profile. However, because lignocellulosic biomass degradation involves overlapping pseudo-component reactions, the selected master-plot model should be interpreted as an apparent macroscopic descriptor rather than as proof of a unique microscopic mechanism [16, 27].

An additional integral comparison can be performed using $g(\alpha)/g(0.5)$, where $g(\alpha) = \int d\alpha/f(\alpha)$. However, in this work, the differential normalized representation based on $f(\alpha)/f(0.5)$ versus α was retained as the primary master-plot framework because it provides a direct comparison of the normalized rate profile. The complete experimental differential and integral master-plot datasets, theoretical model curves, RMSE/SSE/R^2 fitting metrics, and interpolated α_2 audit data are provided as **Online Resource 2**.

2.5 Kinetic modeling

2.5.1 Kissinger peak-based method

The apparent global activation energy associated with the principal devolatilization stage was estimated using the Kissinger peak-based method. This method relates the displacement of the peak temperature with heating rate to the apparent activation energy of a thermally stimulated process. It is widely used in thermal analysis because of its simplicity, but it provides a single global activation energy and should therefore be interpreted cautiously for multi-step biomass degradation processes [12, 15, 16].

The Kissinger equation was applied according to Eq. 13:

$$\ln\left(\frac{\beta}{T_p^2}\right) = \ln\left(\frac{AR}{E_a}\right) - \frac{E_a}{RT_p} \quad (13)$$

where T_p is the DTG peak temperature corresponding to the maximum decomposition rate, β is the heating rate, A is the apparent pre-exponential factor, E_a is the apparent activation energy, and R is the universal gas constant. Linear regression of $ln(\beta/{T_p}^2)$ versus $1/T_p$ yielded E_a from the slope

$-E_a/R$, while the intercept was used to estimate the apparent pre-exponential factor. Because the Kissinger method assumes a dominant peak process, its result was used here as a global kinetic reference rather than as a complete description of the conversion-dependent degradation mechanism [15].

2.5.2 Flynn–Wall–Ozawa (FWO) isoconversional method

Conversion-dependent activation energies were determined using the integral Flynn–Wall–Ozawa (FWO) isoconversional method. Isoconversional methods estimate the apparent activation energy at fixed conversion levels without requiring the prior selection of a specific reaction model. This feature is particularly useful for heterogeneous lignocellulosic biomass, where different pseudo-components and secondary reactions may dominate at different conversion degrees [13, 30, 16].

The FWO method was applied according to Eq. 14:

$$\log_{10}(\beta) = C(\alpha) - 0.4567\frac{E_\alpha}{RT} \quad (14)$$

where E_a is the apparent activation energy at a fixed conversion degree α, $C(\alpha)$ is a conversion-dependent constant, R is the universal gas constant, and T is the absolute temperature. Values of E_α were obtained from the slopes of the linear plots of $log_{10}(\beta)$ versus $1/T$ at constant conversion levels. Because FWO is an integral method, it tends to smooth local fluctuations in the rate signal and is therefore useful as a complementary approach to differential isoconversional analysis [16].

2.5.3 Friedman differential isoconversional method

The Friedman differential isoconversional method was also applied to determine conversion-dependent activation energies directly from the instantaneous reaction rate. Unlike integral methods, the Friedman approach uses the logarithm of the conversion rate at fixed conversion and is consequently more sensitive to local variations in the DTG-derived rate signal. This sensitivity can be advantageous for identifying kinetic heterogeneity, but it also requires careful data smoothing and conversion-window selection when applied to noisy or overlapping thermal events [14, 16].

The Friedman method was applied according to Eq. 15:

$$\ln\left(\frac{d\alpha}{dt}\right) = \ln[Af(\alpha)] - \frac{E_\alpha}{RT} \quad (15)$$

where $d\alpha/dt$ is the conversion rate, A is the apparent pre-exponential factor, $f(\alpha)$ is the differential reaction model, E_a is the apparent activation energy at fixed conversion, R is the universal gas

405 constant, and T is the absolute temperature. Activation energies were calculated from the slopes of
406 $ln(d\alpha/dt)$ versus $1/T$ at each conversion level. The combined use of FWO and Friedman methods
407 enabled comparison between integral and differential isoconversional estimates and supported the
408 identification of conversion-dependent mechanistic transitions during the active devolatilization of
409 chontaduro rachis. Detailed FWO and Friedman activation energies, regression-quality values, shift
410 factors, reconstruction equations, and model-ranking summaries are provided as **Online Resource 2**.

411

412 **2.5.4 Apparent activation thermodynamics**

413 Apparent activation thermodynamic parameters were estimated from the kinetic outputs to provide
414 complementary information on the energetic requirements and structural changes associated with
415 rachis devolatilization. The approach was based on the Eyring transition-state approximation, which
416 has been widely used to relate Arrhenius kinetic parameters with activation enthalpy, entropy, and
417 Gibbs free energy in thermal decomposition and pyrolysis processes [31, 32].

418 Assuming apparent first-order decomposition behavior, the activation enthalpy was calculated
419 according to Eq. 16:

420

421 $$\Delta H^{\ddagger} \approx E_a - RT \quad (16)$$

422

423 where $\Delta H\ddagger$ is the apparent activation enthalpy, E_a is the apparent activation energy, R is the
424 universal gas constant, and T is the absolute temperature.

425 The activation entropy was estimated from the relationship between the apparent pre-exponential
426 factor and transition-state theory, according to Eq. 17:

427

428 $$A \approx \frac{k_B T}{h} \exp\left(\frac{\Delta S^{\ddagger}}{R}\right) \quad (17)$$

429

430 where k_B is the Boltzmann constant and h is Planck's constant, T is the absolute temperature, and
431 $\Delta S\ddagger$ is the apparent activation entropy.

432 Finally, the Gibbs free energy of activation was determined according to Eq. (18).

433

434 $$\Delta G^{\ddagger} = \Delta H^{\ddagger} - T\Delta S^{\ddagger} \quad (18)$$

435

436 where $\Delta G\ddagger$ is the apparent Gibbs free energy of activation. These thermodynamic descriptors were
437 interpreted as apparent parameters because lignocellulosic biomass decomposition involves
438 overlapping pseudo-component reactions, transport effects, and secondary char-forming processes.

Therefore, the calculated $\Delta H\ddagger$, $\Delta S\ddagger$, and $\Delta G\ddagger$ values were used to support comparative interpretation of energetic feasibility and structural organization during active devolatilization rather than to define a unique elementary reaction mechanism [16, 31].

2.6 Differential scanning calorimetry (DSC)

Differential scanning calorimetry (DSC) analyses were performed using a TA Instruments Q2000 thermal analyzer under a nitrogen atmosphere with a constant purge flow of 50 mL min^{-1}. Approximately 5–10 mg of *Bactris gasipaes* Kunth rachis powder was hermetically sealed in aluminum pans and heated from −55 to 500 °C at 10 °C min^{-1}. Heat-flow signals were recorded in W g^{-1} as a function of temperature. DSC was used as a complementary technique to TGA/DTG because it enables the identification of endothermic and exothermic events associated with water removal, structural relaxation, devolatilization, condensation, and carbonization processes in biomass thermal conversion [33, 21].

The raw DSC temperature–heat-flow dataset and the corresponding DSC profile are provided as Online Resource 1 together with the raw TGA/DTG and EGA-MS datasets. Glass-transition-like behavior, when detectable, was estimated from the dominant inflection in the low-temperature region, whereas broader endothermic and exothermic events were evaluated through baseline-corrected enthalpy integration. Biomass thermograms commonly exhibit broad and overlapping transitions rather than sharp events because lignocellulosic matrices contain heterogeneous cellulose, hemicellulose, lignin, extractive, proteinaceous, and mineral fractions [6, 8].

The transition enthalpy was calculated according to Eq. 19

$$\Delta H = \frac{1}{\beta}\int_{T_1}^{T_2}(\dot{q} - \dot{q}_{baseline})\,dT \tag{19}$$

where ΔH corresponds to the transition enthalpy, $\dot{q}$ is the measured heat-flow signal, $\dot{q}_{baseline}$ represents the corrected thermal baseline, β is the heating rate, and T_1 and T_2 define the integration limits associated with each thermal event.

The DSC thermograms were interpreted jointly with TGA/DTG and EGA-MS profiles to establish energetic and mechanistic correlations among dehydration, active devolatilization, exothermic condensation, and progressive carbonization of the lignocellulosic biomatrix. The combined use of mass-loss, heat-flow, and evolved-gas signals is particularly useful for connecting thermal events with chemical conversion pathways in biomass feedstocks [34, 33, 10].

2.7 Evolved-gas analysis by mass spectrometry (EGA-MS)

Evolved-gas analysis by mass spectrometry (EGA-MS) was performed using a TA Instruments Q500 thermogravimetric analyzer coupled to a TA Instruments Discovery MS system. The analyses were carried out under nitrogen atmosphere with a constant flow rate of 50 mL min^{-1}. Approximately 5–

10 mg of chontaduro rachis powder was placed in alumina crucibles and heated under non-isothermal conditions. EGA-MS was used because coupling TGA with mass spectrometry enables temperature-resolved monitoring of volatile species released during thermal decomposition, thereby providing chemical information complementary to mass-loss and DTG signals [10, 9, 11].

Temperature-resolved ion-current intensities were continuously monitored for selected mass-to-charge ratios (m/z) used as diagnostic volatile markers during thermal decomposition. These signals were interpreted as tentative indicators of volatile evolution, including water-related fragments, carbon oxides, hydrocarbon fragments, and nitrogen-containing species. This approach is consistent with previous EGA studies showing that on-line MS detection can help associate DTG events with dehydration, decarboxylation, deamination, cracking, and secondary char-reorganization pathways [10, 11].

The evolved-gas profiles were correlated with DTG signals to evaluate relationships among volatile release, devolatilization behavior, and conversion-dependent thermal decomposition pathways. The temperature-resolved EGA-MS ion-current data for the monitored m/z signals, together with the raw TGA/DTG and DSC datasets used for cross-comparison, are provided as **Online Resource 1**.

2.8 Statistical and multivariate analysis

Statistical analysis included two-way analysis of variance (ANOVA) applied to devolatilization temperatures $\left(T_{\alpha_2}\right)$, considering heating rate (β) and conversion degree (α_2) as fixed factors, including their interaction effects. Pearson correlation analysis was performed between DTG profiles obtained at 10 °C·min^{-1} and the corresponding evolved-gas ion-current signals within the 25–500 °C interval. In addition, principal component analysis (PCA) and hierarchical clustering analysis using Ward's method were conducted on integrated thermoanalytical descriptors derived from TGA, DSC, and EGA-MS datasets to evaluate multivariate relationships among thermal, kinetic, and volatile-evolution features.

2.9 Agroindustrial operational validation of the kinetic treatment

To assess the practical applicability of the kinetic treatment, a conversion–temperature map based on the stage-normalized conversion α_2 was used to define thermal-processing targets for chontaduro rachis valorization. Three target conversions were selected within the active devolatilization region: α_2 = 0.50, 0.70, and 0.90, representing mild devolatilization, torrefaction-like treatment, and advanced carbon-enrichment, respectively. These severity levels are consistent with torrefaction and mild carbonization approaches, where increasing treatment severity generally promotes volatile removal, fixed-carbon enrichment, and improved solid-product stability [35, 36, 37].

Target temperatures were obtained from the interpolated $T\alpha_2(\beta)$ curves at the reference heating rate of 10 °C min^{-1}, corresponding to approximately 233.68 °C, 239.96 °C, and 248.61 °C for α_2 = 0.50, 0.70, and 0.90, respectively. Dried rachis biomass was thermally treated under inert atmosphere at each predicted temperature and immediately cooled under inert gas. The response variables included solid yield, mass loss, experimental α_2, volatile-matter reduction, ash enrichment, fixed-carbon

enrichment, and higher heating value when available. The observed α_2 values were compared with the target values using prediction error, absolute error, mean absolute error, and root-mean-square error. This operational validation was used as a process-oriented assessment of whether the TGA-derived conversion map can guide temperature selection, thermal severity, and product targeting for agroindustrial biomass conversion [8, 33]. The operational validation conditions proposed for chontaduro rachis thermal valorization are summarized in **Table 2**.

[Insert Table 2 here]

Table 2. Proposed operational validation matrix for chontaduro rachis thermal valorization

Validation condition	**Target α_2**	**Operational meaning**	**Predicted temperature source**	**Response variables**
Mild treatment	0.50	Partial active devolatilization	$T\alpha_2$ at selected β	Solid yield, mass loss, α_2 error
Intermediate treatment	0.70	Torrefaction-like transformation	$T\alpha_2$ at selected β	Volatile reduction, fixed-carbon enrichment
Advanced treatment	0.90	Near-complete active devolatilization	$T\alpha_2$ at selected β	Carbon-enriched solid, residual volatile matter

3. Results and Discussion

The proximate composition results used as the compositional basis for interpreting the thermal behavior of chontaduro rachis powder are presented in **Table 3**.

[Insert Table 3 here]

Table 3. Proximal composition of the chontaduro rachis powder (wet basis, % w/w)

Component	**Content (%)**
Moisture	5.2 ± 0.2
Protein	8.6 ± 0.3
Lipid	3.1 ± 0.2
Ash	7.4 ± 0.2
Total dietary fiber	45.7 ± 1.2
Carbohydrates (by difference)	30.0 ± 1.4

Values are expressed as mean ± SD (n = 3).

The compositional profile helped explain the main thermoanalytical features observed during multi-rate TGA/DTG, DSC, and EGA-MS analyses. The initial moisture content (5.2 ± 0.2%) was

consistent with the first mass-loss region detected between 25 and 150 °C, which is commonly associated with the release of free and weakly bound water from lignocellulosic biomass. This dehydration event is also expected to correspond to an endothermic DSC signal, reflecting the energy required for water desorption and evaporation [6, 10].

The high dietary fiber and carbohydrate contents were consistent with the pronounced mass loss observed during the active devolatilization stage. In lignocellulosic biomass, this region generally results from overlapping degradation of hemicellulose, cellulose, extractives, and other thermally labile organic fractions, while lignin contributes to broader and slower decomposition over an extended temperature range. Previous TGA-based studies and reviews have shown that the thermal degradation of biomass is usually multistage, with hemicellulose decomposing at lower temperatures, cellulose contributing strongly to the main DTG peak, and lignin degrading gradually across a wider thermal domain [38, 6, 39].

The protein content (8.6 ± 0.3%) may also contribute to the release of nitrogen-containing volatile fragments during the primary devolatilization regime. In this study, the detection of m/z 17 should be interpreted cautiously as an ammonia-related or nitrogen-containing signal, because this ion can also be affected by overlapping fragment contributions in EGA-MS. Therefore, its assignment should be considered tentative and discussed together with the DTG maximum and the full evolved-gas profile rather than as an isolated molecular identification [10, 11].

Finally, the ash fraction (7.4 ± 0.2%) and the formation of thermally stable carbonaceous structures during lignin-rich condensation and aromatization processes help explain the residual mass observed at 700 °C. In biomass pyrolysis, inorganic ash can remain as a stable residue, whereas fixed carbon and char formation are strongly influenced by lignin content, mineral matter, heating history, and secondary reactions. These features support the potential of chontaduro rachis as a precursor for carbon-enriched solids, biochar-like materials, or thermally upgraded biomass products, although this application should be further confirmed through solid-product characterization such as fixed carbon, HHV, elemental analysis, FTIR, XRD, or surface-property measurements [39, 38, 2].

3.2 Multi-rate TGA/DTG

As shown in **Fig. 2**, the multi-rate thermogravimetric and derivative thermogravimetric profiles of chontaduro (*Bactris gasipaes* Kunth) rachis powder revealed a clearly staged thermal decomposition pattern under non-isothermal conditions. The continuous TGA curves showed the progressive decrease in residual mass with temperature, whereas the dotted DTG curves identified the main degradation-rate events at the four heating rates evaluated: 5, 10, 15, and 20 °C min^{-1}. The vertical dashed lines in **Fig. 2** delimit three main thermal regions: Stage 1, associated mainly with dehydration; Stage 2, corresponding to active devolatilization; and Stage 3, related to progressive carbonization and secondary cracking. This multi-stage profile is consistent with the overlapping decomposition of lignocellulosic pseudo-components, including hemicellulose-rich domains, cellulose-rich fractions, lignin-derived structures, extractives, and mineral-associated residues [38, 6, 39].

The first thermal region, extending approximately from 25 to 150 °C in **Fig. 2**, corresponded mainly to dehydration and physical desorption phenomena. Across the four heating rates, the initial mass loss was consistent with the experimentally determined moisture content of the rachis powder. This stage is commonly associated with the release of free water and weakly bound water retained within hydrogen-bonded polysaccharide structures. The low-temperature DTG signal observed in **Fig. 2** also suggests that moisture removal occurred before the onset of the dominant organic devolatilization stage. Water release can influence the early DTG response by modifying heat transfer, local matrix relaxation, and volatile diffusion pathways during subsequent thermal conversion [6, 40].

Following dehydration, the rachis entered the active devolatilization region, visually identified as Stage 2 in **Fig. 2**. This region represented the dominant mass-loss event and was characterized by intense DTG peaks centered within the main decomposition interval. The onset temperature of this stage remained relatively stable at approximately 162–164 °C, suggesting that the initiation of active devolatilization was mainly associated with the most thermally labile constituents of the biomass. These may include hemicellulosic, pectic, extractive, and amorphous carbohydrate domains; however, such assignments should be considered tentative unless supported by direct structural fractionation. Previous TGA-based studies indicate that hemicellulose and related xylan-rich fractions generally decompose earlier than cellulose and contribute substantially to early volatile release in lignocellulosic biomass [41, 38, 6].

In contrast to the nearly constant onset temperature, the maximum degradation temperature shifted to higher values as the heating rate increased. As observed in **Fig. 2**, the dominant DTG maximum moved from approximately 229.3 °C at 5 °C min^{-1} to 245.5 °C at 20 °C min^{-1}. This rightward displacement is characteristic of non-isothermal biomass degradation and reflects the combined influence of thermal lag, reduced residence time at intermediate temperatures, and heat/mass-transfer limitations at higher heating rates. The increase in DTG peak intensity also indicates a more concentrated release of volatile matter under faster heating. Such heating-rate dependence supports the need for multi-rate kinetic analysis rather than interpretation from a single thermal profile [39, 8].

After the principal devolatilization interval, the material entered Stage 3, extending from approximately 277 °C to 700 °C, as shown in **Fig. 2**. This stage was characterized by slower but sustained mass loss and secondary DTG features, indicating progressive carbonization, aromatic rearrangement, and secondary cracking of the residual matrix. The presence of secondary DTG peaks or shoulders in this high-temperature domain suggests that the intermediate char remained thermally reactive rather than behaving as an inert residue. This behavior is consistent with the broad degradation range of lignin-derived aromatic structures and with secondary reactions involving active char, tar intermediates, and residual oxygenated functionalities [42, 38, 39].

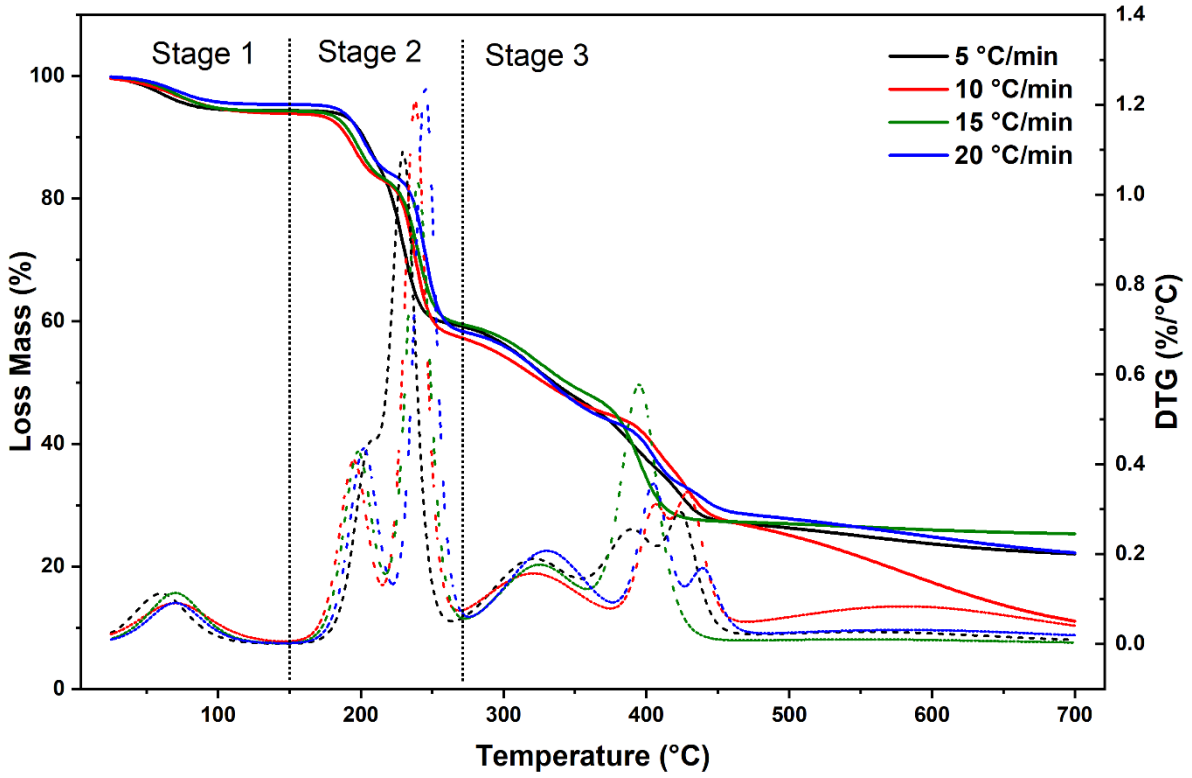


Fig 2 Thermogravimetric and derivative thermogravimetric profiles of chontaduro (*Bactris gasipaes* Kunth) rachis powder at different heating rates: 5, 10, 15, and 20 °C min^{-1}. Continuous lines represent residual mass, and dotted lines represent DTG signals. Vertical dashed lines delimit the main thermal regions: Stage 1, dehydration; Stage 2, active devolatilization; and Stage 3, progressive carbonization and secondary cracking

3.3 TGA/DTG quantitative descriptors

The characteristic thermogravimetric descriptors summarized in **Table 4** provide quantitative evidence of the multi-stage and heating-rate-dependent decomposition behavior of chontaduro rachis. The active devolatilization onset temperature, $T_{on,2}$, varied only slightly from 161.9 to 164.0 °C across the four heating rates, indicating that the initiation of the main devolatilization event was relatively stable. This limited variation suggests that the onset of active decomposition was mainly associated with the most thermally labile domains of the biomass, including hemicellulose-rich, pectic, extractive, and amorphous carbohydrate fractions. However, these assignments should be interpreted as tentative unless supported by direct structural fractionation. Similar early decomposition behavior has been reported for xylan/hemicellulosic fractions and lignocellulosic biomass under non-isothermal pyrolysis conditions [41, 6, 38].

In contrast, the maximum degradation temperature, $T_{max,2}$, exhibited a clear rightward displacement as the heating rate increased, shifting from 229.3 °C at 5 °C min^{-1} to 245.5 °C at 20 °C min^{-1}. This behavior is characteristic of non-isothermal biomass degradation and reflects the combined effects of

thermal lag, reduced residence time, and heat/mass-transfer limitations at higher heating rates. Under faster heating, the biomass particles experience less time for heat equilibration and volatile diffusion, causing the apparent maximum degradation rate to occur at higher temperatures. This heating-rate-induced peak displacement has been widely reported in biomass pyrolysis and is one of the main reasons why multi-rate datasets are required for reliable kinetic interpretation [39, 8].

The DTG peak intensity also changed with heating rate, reaching values between 1.0256 and 1.2344% °C^{-1} during the active devolatilization stage. The highest DTG intensity observed at 20 °C min^{-1} indicates a more concentrated volatile release under faster heating. This response can be attributed to the compression of decomposition events into a narrower temperature interval, together with accelerated devolatilization of carbohydrate-rich fractions. Nevertheless, the non-monotonic value observed at 15 °C min^{-1} suggests that the DTG response is not controlled only by heating rate but also by overlapping pseudo-component reactions, local heat transfer, and volatile-release dynamics. This reinforces the interpretation that chontaduro rachis decomposition is not a single-step reaction but a sequence of partially overlapping processes [38, 16, 8].

The active devolatilization mass loss, Δm_2, ranged from 34.829 to 37.289%, confirming that this stage was the dominant mass-loss event. This mass loss is consistent with the degradation of thermally labile lignocellulosic fractions, particularly hemicellulose-rich and cellulose-rich domains, together with extractives and other volatile-forming organic structures. In biomass TGA studies, hemicellulosic fractions generally contribute to earlier decomposition, cellulose-rich fractions frequently dominate the main DTG peak, and lignin-derived structures decompose over a wider temperature interval, contributing to secondary shoulders and residual char formation [6, 38, 42].

After the active devolatilization interval, the post-devolatilization mass loss from $T_{end,2}$ to 700 °C ranged from 34.012 to 46.213%, showing that the residual matrix remained thermally reactive during the high-temperature stage. This behavior is consistent with secondary cracking, aromatization, condensation, and progressive degradation of lignin-derived and char-forming structures. Lignin pyrolysis is known to involve broad thermal degradation and multiple parallel reactions, including demethoxylation, demethylation, decarboxylation, depolymerization, recombination, and char formation [42, 43].

The residual mass at 700 °C, calculated from the cumulative mass losses in Table 4, ranged approximately from 11.2 to 25.4%. This residue likely reflects the combined contribution of inorganic ash and thermally stabilized carbonaceous structures generated during late-stage condensation and aromatization. However, the residual mass did not vary linearly with heating rate: the highest calculated residue was observed at 15 °C min^{-1}, while the lowest occurred at 10 °C min^{-1}. Therefore, the data suggest that residual char formation was influenced by competing effects of volatile release, secondary condensation, mineral matter, and heating history, rather than by heating rate alone. Alkali and alkaline earth metals present in biomass ash can catalyze decomposition reactions, shift characteristic pyrolysis temperatures, and modify activation energies, which may partly explain differences in residual mass and secondary degradation behavior [44, 45, 39].

[Insert Table 4 here]

669 **Table 4**. Characteristic TGA/DTG descriptors and mass-loss distribution of chontaduro rachis at
670 different heating rates

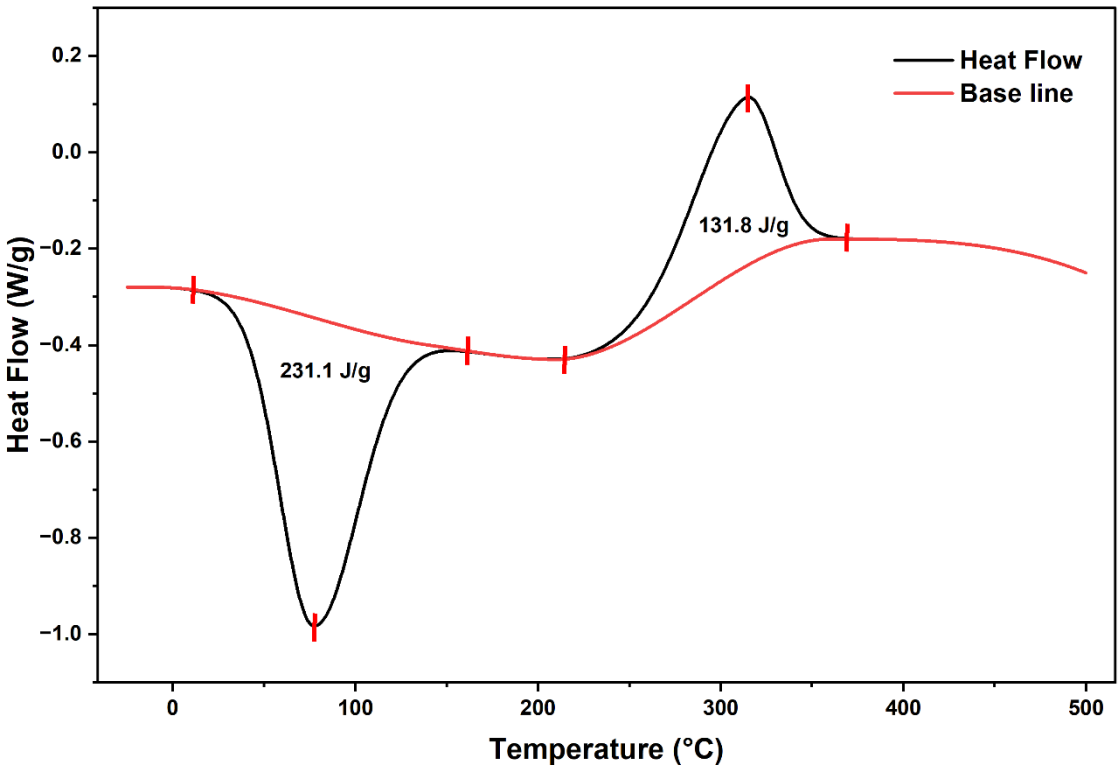
β (°C/min)	m_0 (%)	Mass Loss 5–150°C (%)	$T_{on\,2}$ (°C)	$T_{\max\,2}$ (°C)	$T_{end\,2}$ (°C)	DTG max 2 (%/°C)	Δm_2 (%)	Δm (T_{end} →700°C) (%)	Peak sec 1 T (°C)	DTG 1	Peak sec 2 T (°C)	DTG 2
5	99.675	5.313	163.501	229.259	264.429	1.0949	34.829	37.452	422.695	0.2936	390.230	0.2556
10	99.612	5.702	163.413	237.375	271.192	1.2051	36.514	46.213	428.106	0.3381	321.242	0.1572
15	99.831	5.523	161.889	240.080	273.898	1.0256	34.912	34.012	394.289	0.5770	325.301	0.1767
20	99.865	4.497	164.017	245.491	276.603	1.2344	37.289	35.802	405.110	0.3571	330.711	0.2076

671

672 **3.4 DSC energetics support dehydration followed by condensation/aromatization**

673 Differential scanning calorimetry (DSC) provided the enthalpic counterpart to the mass-loss events
674 observed by TGA/DTG, allowing endothermic and exothermic thermal events to be distinguished
675 during the thermal conversion of chontaduro rachis. As shown in **Fig. 3**, the DSC profile exhibited
676 two broad thermal events rather than sharp melting or crystallization peaks, which is consistent with
677 the heterogeneous and partially amorphous nature of lignocellulosic biomass. Similar broad DSC
678 responses have been reported for lignocellulosic wastes and biomass feedstocks, where cellulose,
679 hemicellulose, lignin, extractives, water, and mineral constituents contribute to overlapping
680 relaxation, dehydration, degradation, and char-forming processes [46, 33].

681



682

683 **Fig 3** Differential scanning calorimetry profile of chontaduro (*Bactris gasipaes* Kunth) rachis powder.
684 The black curve represents heat flow and the red curve represents the baseline used for enthalpy
685 integration

686

687 The first thermal event was an endothermic peak with an onset temperature of 26.67 °C, a peak
688 temperature of 76.74 °C, and an integrated enthalpy of 231.1 J g^{-1} (Table 5). This event is mainly
689 attributed to the evaporation of free water and the desorption of weakly bound water retained within
690 the porous polysaccharide-rich network. Its position agrees with the first TGA mass-loss region and
691 supports the interpretation that the low-temperature thermal response of the rachis is dominated by
692 dehydration. Comparable behavior is commonly observed in biomass thermograms, where water
693 removal precedes the main devolatilization stage and appears as an endothermic process in DSC or
694 TG–DSC measurements [47, 34].

695 The second thermal event appeared as a broad exothermic peak with an onset temperature of 243.21
696 °C, a peak temperature of 313.74 °C, and an integrated enthalpy of 131.8 J g^{-1} (**Table 5**). This
697 temperature region overlaps with the transition from active devolatilization to secondary
698 decomposition observed in TGA/DTG. Therefore, the exothermic response is consistent with
699 concurrent condensation, recombination, aromatization, and char-forming reactions occurring after
700 the initial cleavage of thermally labile polysaccharide structures. In biomass pyrolysis, primary
701 degradation may include both endothermic bond-cleavage processes and exothermic secondary
702 reactions, particularly when tar recombination, char formation, and aromatization become important
703 [47].

The integration of DSC with TGA/DTG and EGA-MS strengthens the mechanistic interpretation of these events. The low-temperature endothermic region coincided with moisture-related signals, mainly m/z 18, whereas the higher-temperature exothermic region overlapped with the evolution of CO_2-related, H_2O-related, and organic volatile fragments detected by EGA-MS. However, these assignments should be considered tentative volatile markers rather than definitive molecular identifications, because nominal m/z signals may include overlapping ion fragments. Coupled TGA–DSC–MS and EGA-MS approaches are widely used to connect mass loss, heat flow, and evolved-gas formation during biomass pyrolysis, but interpretation requires caution when assigning individual ions to specific molecules [10, 9, 11].

[Insert Table 5 here]

Table 5. Summary of DSC thermal parameters and associated phenomena

Parameter/property	**Peak 1**	**Peak 2**
Nature of phenomenon	Endothermic	Exothermic
Peak temperature, T_p	76.74 °C	313.74 °C
Onset temperature, T_{on}	26.67 °C	243.21 °C
Transition enthalpy, ΔH	231.1 J g^{-1}	131.8 J g^{-1}
Associated EGA-MS markers	Moisture-related signal, mainly m/z 18; possible overlapping m/z 17 contribution	CO_2-related m/z 44, H_2O-related m/z 18, and organic volatile fragments, including m/z 15, 26, 27, and 29
Main physicochemical interpretation	Surface dehydration, evaporation of free water, and desorption of weakly bound water	Structural conversion, condensation, secondary reactions, aromatization, and char-forming processes

3.5 EGA-MS fingerprints identify volatile reporters of composition and stages

Unlike standalone thermoanalysis, coupling thermogravimetry with on-line mass spectrometry (EGA-MS) provides temperature-resolved ion-current profiles that can be correlated with macroscopic mass-loss events. As shown in **Fig. 4**, the TGA profile and selected m/z signals exhibited synchronized maxima during the active devolatilization region, indicating that specific volatile markers were released concurrently with the principal degradation event. However, the assignments of individual ions should be interpreted as tentative volatile markers rather than unequivocal molecular identifications, because several species may contribute to the same nominal m/z signal in electron-impact mass spectrometry [10, 9, 11].

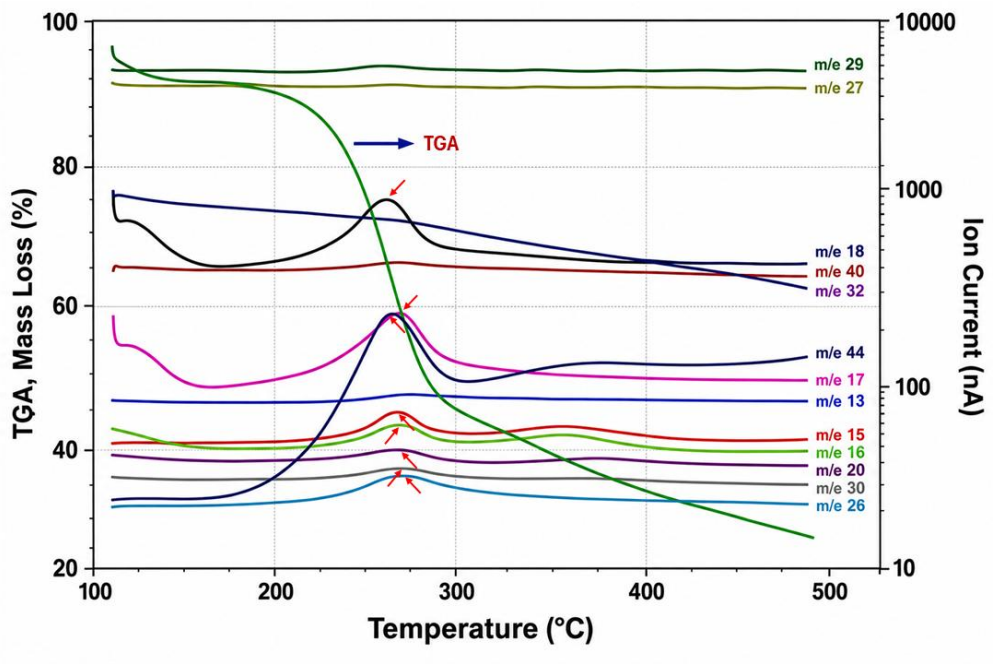


Fig 4 Coupled TGA–EGA-MS profile of chontaduro (*Bactris gasipaes* Kunth) rachis powder. The TGA curve is shown together with temperature-resolved ion-current signals for selected m/z values monitored during thermal decomposition

During the active devolatilization stage, centered near 233–235 °C, the evolved-gas profile was dominated by signals at m/z 44, m/z 18, and m/z 17. The m/z 44 signal, mainly associated with CO_2-related fragments, showed the strongest association with the principal DTG event ($r \approx 0.835$), suggesting that decarboxylation reactions were important during the main degradation stage. Such CO_2 evolution is consistent with the thermal decomposition of oxygenated carbohydrate structures, including hemicellulosic, uronic-acid-containing, and pectic-like domains commonly present in lignocellulosic biomass and food-derived residues [48, 6].

The m/z 18 signal, mainly associated with H_2O-related fragments, reached its maximum close to the same temperature region, supporting the occurrence of dehydration reactions during active devolatilization. This water evolution should not be interpreted only as residual moisture loss, because at this temperature it may also arise from chemical dehydration, polysaccharide breakdown, and condensation reactions within the lignocellulosic matrix. Similar behavior has been reported in coupled thermal-analysis studies of biomass, where H_2O and CO_2 are frequently detected as major evolved species during pyrolysis and devolatilization [10, 34, 6].

The m/z 17 signal was also synchronized with the main devolatilization region and may be associated with NH_3-related or amine-derived fragments generated from nitrogen-containing constituents, including residual proteinaceous structures. Nevertheless, this assignment must be considered tentative because m/z 17 can also include contributions from OH^+ fragments derived from water. Therefore, the signal is best described as a nitrogen-containing/ammonia-related marker only when interpreted together with the full EGA-MS profile and the proximate protein content [10, 9, 11].

In the high-temperature region above 400 °C, a different set of ion-current maxima became more evident, including m/z 15, m/z 27, and m/z 29. These signals are consistent with the progressive fragmentation of hydrocarbon, oxygenated, and nitrogen-containing structures during secondary cracking and char reorganization. Lignin-derived structures can decompose over a broad temperature interval and undergo demethoxylation, demethylation, decarboxylation, decarbonylation, radical recombination, and char-forming reactions, which may give rise to delayed volatile emissions and persistent carbonaceous residues [42, 43].

The delayed maximum of m/z 29 near 675.7 °C suggests that late-stage cracking of oxygenated carbonaceous structures occurred after the principal devolatilization event. However, this signal should not be assigned exclusively to CO or CHO^+ without complementary confirmation, because nominal m/z 29 may include multiple fragment contributions. Similarly, m/z 27 may be related to HCN or $C_2H_3^+$-type fragments, but the assignment remains tentative. Overall, the EGA-MS results indicate a thermo-chemical transition from oxygen-rich volatile release during carbohydrate-dominated active devolatilization to delayed fragmentation and reorganization of increasingly aromatized carbonaceous structures at higher temperatures [10, 9, 42]. The dominant evolved MS ions and their tentative mechanistic assignments during chontaduro rachis thermal decomposition are summarized in **Table 6**.

[Insert Table 6 here]

Table 6. Dominant evolved mass spectrometry (MS) ions and their mechanistic assignments during the thermal decomposition of chontaduro rachis

Ion, m/z	**Peak temperature (°C)**	**Tentative evolved species/fragment**	**Mechanistic interpretation**
44	233.3	CO_2-related fragments	Decarboxylation of oxygenated carbohydrate structures, including hemicellulosic, uronic-acid-containing, and pectic-like domains
17	233.3	NH_3-related/amine-derived fragments; possible OH^+ contribution	Tentative marker of nitrogen-containing volatile release; possible overlap with water-derived fragments
18	234.7	H_2O-related fragments	Chemical dehydration and release of structurally bound water during polysaccharide degradation and condensation
15	426.8	CH_3^+-type fragments	Cracking or rearrangement of methyl-bearing intermediates during secondary carbonization

16	466.0	CH_4^+/O-related fragments	Intermediate-to-late hydrocarbon or oxygenated-fragment evolution
32	562.0	O_2/oxygenated fragments; possible background contribution	High-temperature oxygenated signal; assignment should be treated cautiously
40	579.6	Ar^+/Ca-related or background/mineral-associated signal	Possible carrier/background contribution or mineral-associated signal
13	591.8	CH^+-type fragments	Late-stage fragmentation of aromatized hydrocarbon structures
27	614.8	HCN/$C_2H_3^+$-type fragments	Tentative marker of nitrogen-containing or unsaturated hydrocarbon fragmentation during advanced carbonization
29	675.7	CO/CHO^+-type fragments	Late-stage cracking of oxygenated carbonaceous structures and condensed char domains

3.6 Thermal superposition and conversion-dependent shift factors

Fig. 5 shows the conversion-dependent thermal-shift factors, $\Delta T(\alpha_2,\beta)$, calculated relative to the reference heating rate of 10 °C min^{-1} during the active devolatilization stage. The reference curve remains fixed at $\Delta T = 0$, whereas the curves obtained at 5, 15, and 20 °C min^{-1} deviate from zero in a conversion-dependent manner. This behavior indicates that the effect of heating rate cannot be interpreted as a simple uniform horizontal displacement of the active devolatilization profile. Instead, the magnitude and direction of the thermal shift depend on the conversion level, supporting the presence of overlapping and conversion-dependent degradation sub-processes. Such behavior is consistent with ICTAC recommendations, which emphasize that multi-step solid-state processes should be evaluated using conversion-resolved approaches rather than single global descriptors [16].

At low heating rate, the 5 °C min^{-1} curve becomes predominantly negative after the perturbation region, indicating that the same α_2 level was reached at lower apparent temperatures than at the reference heating rate. In contrast, the 20 °C min^{-1} curve remains positive over most of the conversion range, showing that faster heating shifted the apparent conversion temperature upward. This trend is consistent with thermal-lag effects and reduced time for heat and mass-transfer equilibration under faster non-isothermal heating. Similar heating-rate effects have been reported in biomass pyrolysis, where particle properties, heat-transfer limitations, residence time, and heating regime influence the applicability of TGA-derived kinetic parameters [49, 39].

The pronounced deviation around $\alpha_2 \approx 0.30$, particularly for the 5 and 15 °C min^{-1} curves, suggests that the most intense part of active devolatilization involved overlapping sub-processes rather than a single reaction front. This perturbation likely reflects a transition from more labile amorphous

fractions, including hemicellulosic or pectic-like domains, toward more resistant carbohydrate-rich and lignin-associated structures. Previous studies have shown that hemicellulose, cellulose, and lignin contribute differently to biomass pyrolysis and combustion behavior, with partially overlapping but composition-dependent degradation intervals [50, 6].

The non-constant $\Delta T(\alpha_2,\beta)$ profiles support the use of stage-normalized conversion and reinforce the need for isoconversional kinetic analysis. Rather than showing a uniform thermal shift, the curves demonstrate that heating rate interacts with conversion level, reflecting a multi-step devolatilization process controlled by pseudo-component overlap, volatile diffusion, thermal lag, and progressive char-forming transformations. Therefore, Fig. 5 complements the TGA/DTG descriptors and provides a methodological basis for the subsequent master-plot and activation-energy analyses. This interpretation is consistent with recent reviews emphasizing the importance of thermal analysis, kinetic modeling, and volatile-release behavior for understanding biomass conversion from micro- to macro-scale perspectives [51, 8].

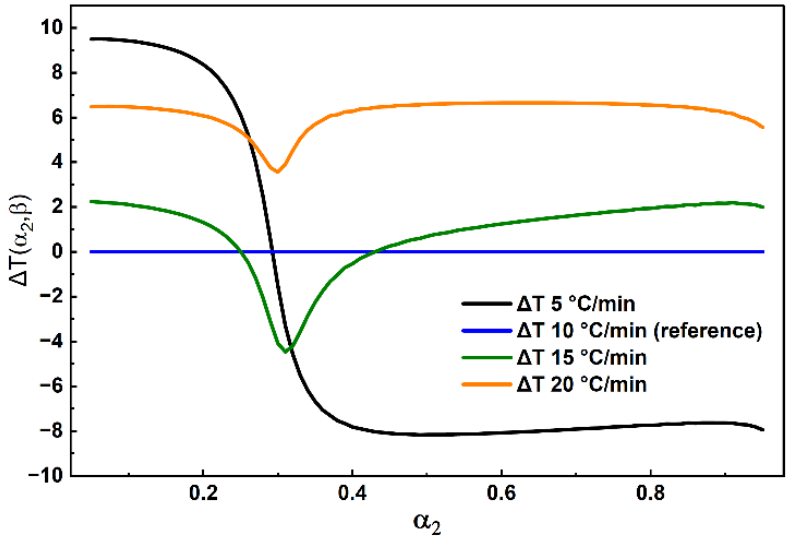


Fig 5 Conversion-dependent thermal-shift factors, $\Delta T(\alpha_2,\beta)$, calculated relative to the reference heating rate of 10 °C min^{-1} during the active devolatilization stage of chontaduro rachis. Positive values indicate that a given α_2 level was reached at a higher temperature than in the reference run, whereas negative values indicate that the same conversion level was reached at a lower temperature

3.7 Master-plot analysis and thermal-shift behavior

A central challenge in non-isothermal solid-state kinetics is determining whether changes in heating rate modify the apparent decomposition pathway or mainly shift the temperature domain in which a similar reaction network occurs. To address this issue, the active devolatilization stage was normalized using $\boldsymbol{\alpha_2}$ and evaluated through the integrated kinetic representation shown in **Fig. 6**. This figure combines differential and integral master plots with conversion-dependent temperature-shift

factors and isoconversional activation-energy trends, allowing the normalized rate behavior to be interpreted together with the evolution of the kinetic barrier. This type of conversion-resolved analysis is consistent with ICTAC recommendations for complex multi-step processes, where global kinetic descriptors may mask overlapping reaction pathways [16].

The differential master plot in **Fig. 6A** provided the most direct model-discrimination evidence because it compared the experimental normalized reaction-rate profile with theoretical $f(\alpha)/f(0.5)$ functions. The experimental curve showed a broad maximum at intermediate-to-advanced conversion and did not follow a simple first-order decay. Among the candidate models, the Avrami–Erofeev-type curves, particularly A3, reproduced the curvature of the experimental profile more closely than the first-order model F1 or the contracting-geometry model R2. Therefore, A3 was retained as the best apparent descriptor of the normalized devolatilization-rate profile. However, this selection should be interpreted as a macroscopic kinetic descriptor rather than definitive proof of a unique microscopic nucleation-growth mechanism, because biomass devolatilization involves overlapping pseudo-component degradation and secondary reactions [28, 27, 29].

The integral master plot in **Fig. 6B** provided complementary information on cumulative conversion behavior. The experimental integral curve increased sharply at higher α_2, indicating that the later part of the active devolatilization stage accumulated conversion more rapidly than several idealized model curves predicted. Because integral master plots are more sensitive to the activation-energy value used to construct the reduced-time scale, **Fig. 6B** was used as supporting evidence rather than as the primary basis for model selection. In this sense, the differential master plot remained the strongest argument for selecting A3 as the most compatible apparent rate descriptor [27].

The temperature-shift factors in **Fig. 6C** and **Table 7** further demonstrated that the heating-rate effect was not a constant horizontal displacement. The 10 °C min^{-1} curve was fixed at ΔT = 0 as the reference, whereas the 5 °C min^{-1} curve remained negative in the interval α_2 = 0.4–0.9, and the 20 °C min^{-1} curve remained positive. This confirms that slower heating reached the same α_2 at lower apparent temperatures, while faster heating shifted the apparent conversion temperature upward. The 15 °C min^{-1} profile was especially informative because ΔT changed from −0.53 °C at α_2 = 0.4 to +2.16 °C at α_2 = 0.9, revealing that the heating-rate effect depended on conversion level. Such non-constant $\Delta T(\alpha_2, \beta)$ behavior is consistent with pseudo-component overlap, thermal lag, volatile-diffusion limitations, and progressive char-forming transformations during biomass conversion [49, 39, 8].

Overall, **Fig. 6A–C** indicates that the active devolatilization stage was sufficiently coherent to justify α_2-based normalization and model comparison, but not simple enough to be represented by a single global reaction. The combined evidence from the master plots and ΔT profiles supports an apparent multi-step pathway in which more labile amorphous constituents dominate the early conversion region, whereas more resistant polysaccharide-rich and lignin-derived structures increasingly influence the response at higher conversion. Similar composition-dependent behavior has been reported for natural fibers and lignocellulosic biomasses, where cellulose, hemicellulose, and lignin contents strongly affect pyrolysis, combustion, char formation, and kinetic response [50, 6, 7].

[Insert Table 7 here]

Table 7. Temperature shift factors (ΔT) relative to the reference heating rate of 10 °C·min^{-1} during the active devolatilization stage (α_2 = 0.4–0.9).

β (°C/min)	ΔTmean (°C)	ΔT at α_2=0.4	ΔT at α_2=0.7	ΔT at α_2=0.9
5	−7.89	−7.82	−7.92	−7.64
10	0	0	0	0
15	1.19	−0.53	1.63	2.16
20	6.49	6.27	6.64	6.21

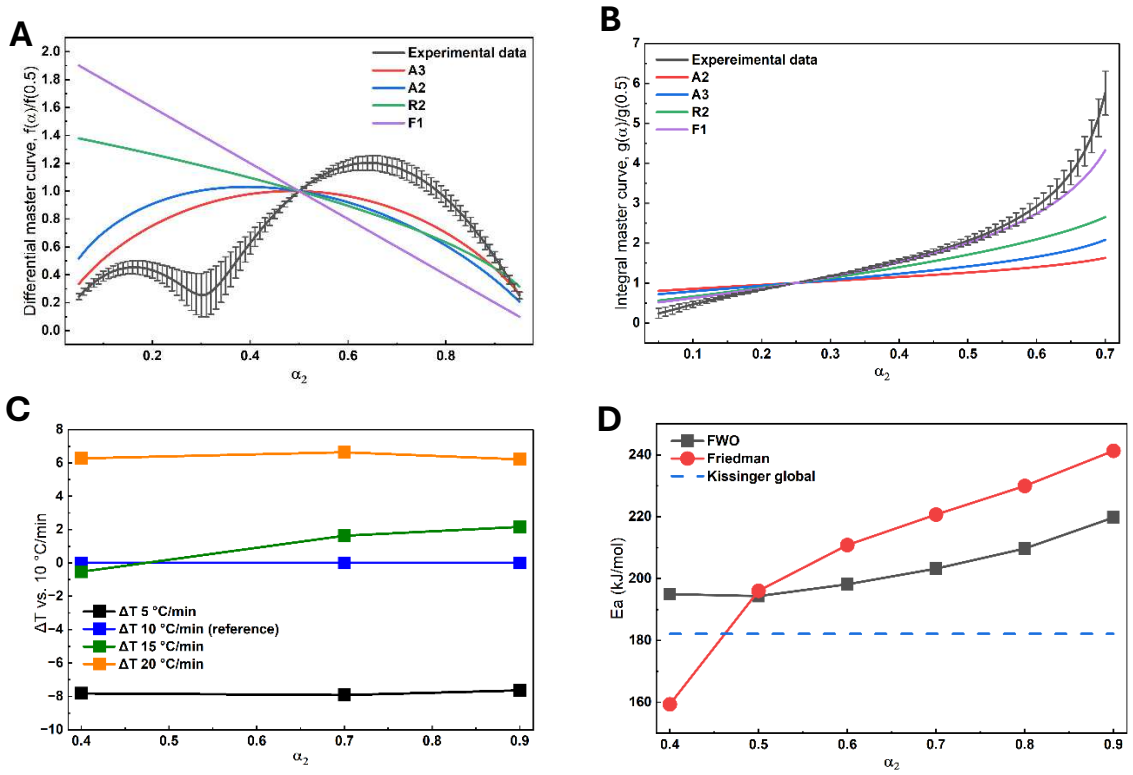


Fig 6 Integrated kinetic analysis of the active devolatilization stage of chontaduro rachis: (A) differential master plot, (B) integral master plot, (C) conversion-dependent thermal-shift factors (ΔT), and (D) conversion-dependent activation energy obtained from FWO and Friedman methods with the Kissinger global activation energy as reference

3.8 Isoconversional kinetics and thermodynamics: conversion-dependent activation energy reveals mechanistic transitions

Following ICTAC recommendations for complex solid-state processes, the activation energy was evaluated by combining a global peak-based method with model-free isoconversional approaches. The Kissinger method yielded a global apparent E_a of 182.05 kJ mol^{-1} with $R^2 = 0.979$, representing an average kinetic barrier around the dominant DTG maximum. However, this single value cannot describe the conversion-dependent evolution of the active devolatilization stage, as shown by the Flynn–Wall–Ozawa (FWO) and Friedman profiles in Fig. 6D. This limitation is well recognized because Kissinger-type peak methods may provide nearly linear plots even when the underlying process is multi-step and the activation energy varies with conversion [12, 15, 16].

As shown in **Fig. 6D** and **Table 8**, E_a increased with conversion for both isoconversional methods. The FWO values increased moderately from 194.95 to 219.72 kJ mol^{-1} between $\alpha = 0.4$ and 0.9, whereas Friedman values increased more strongly from 159.35 to 241.30 kJ mol^{-1} over the same interval. The global Kissinger value lies between the low- and high-conversion Friedman values and below the high-conversion FWO/Friedman region, confirming that Kissinger provides a useful global reference but masks the progressive increase in kinetic resistance during conversion. Isoconversional approaches are particularly useful for heterogeneous biomass because they estimate $E_a(\alpha)$ without forcing the process into a single predefined reaction model [13, 30, 14].

The comparatively low Friedman E_a at $\alpha = 0.4$ is consistent with early decomposition of more labile amorphous constituents, such as hemicellulosic/pectic-like domains, extractives, and side-group elimination reactions. At higher conversions, especially $\alpha \geq 0.7$, both FWO and Friedman indicated larger activation barriers, which is compatible with the increasing contribution of more resistant cellulose-rich and lignin-derived aromatic structures. This interpretation is consistent with previous studies showing that hemicellulose, cellulose, and lignin exhibit distinct but overlapping decomposition domains and that lignin-rich structures can contribute to broader, higher-temperature degradation and char formation [6, 50, 42].

The differences between FWO and Friedman should be interpreted as methodological complementarity rather than contradiction. Friedman is a differential method and is therefore more sensitive to local variations and noise in DTG-derived rates, whereas FWO is an integral method and tends to smooth local fluctuations. The high R^2 values for Friedman and the improved FWO regression quality after $\alpha = 0.5$ support the reliability of the selected conversion interval, while the lower FWO R^2 at $\alpha = 0.4$ suggests that low-conversion data may still be affected by overlapping dehydration, relaxation, or early devolatilization effects. The need for careful conversion-window selection and cautious interpretation of derivative-based kinetic data is emphasized in ICTAC recommendations and kinetic-analysis reviews [16, 52].

The apparent pre-exponential factors derived from Friedman parameters increased with conversion, from $lnA = 32.90$ at $\alpha = 0.4$ to $lnA = 51.94$ at $\alpha = 0.9$ (**Table 9**). This trend is consistent with an apparent kinetic compensation behavior, but it should be discussed cautiously because lnA depends on the regression intercept, the assumed apparent reaction model, and the quality of the derivative rate data. Therefore, lnA should be interpreted as an apparent descriptor of structural reorganization and changing reaction complexity during conversion, rather than as an independently measured molecular frequency factor. Kinetic compensation and distributed reactivity are commonly encountered in biomass pyrolysis because multiple pseudo-components and secondary reactions contribute simultaneously to the observed mass-loss rate [53, 54, 8].

The activation thermodynamic parameters were estimated at the mean peak temperature using the Eyring–Arrhenius formalism. The analysis yielded an apparent activation enthalpy, ΔH ‡, of 177.80 kJ mol^{-1}, an apparent Gibbs free energy of activation, ΔG ‡, of 123.54 kJ mol^{-1}, and an apparent activation entropy, ΔS ‡, of 106.13 J mol^{-1} K^{-1}. The positive ΔG ‡ indicates a positive activation barrier that must be overcome for devolatilization to proceed under the imposed thermal program, while the positive ΔS ‡ suggests a more disordered activated state relative to the condensed solid matrix. This behavior is consistent with bond cleavage, volatile formation, expansion of reactive intermediates, and progressive structural opening during biomass thermal conversion. Thermodynamic activation parameters should nevertheless be interpreted as apparent quantities because biomass devolatilization is not an elementary reaction but a composite process involving overlapping pseudo-components and secondary char-forming reactions [31, 32, 16].

Collectively, **Fig. 6D**, **Table 8**, **Table 9**, and the activation thermodynamic descriptors reinforce the conclusion that chontaduro rachis devolatilization proceeds through an apparent multi-step process. The increasing $E_a(\alpha)$ trend, non-uniform thermal shifts, and compensation-like increase in lnA indicate a transition from labile carbohydrate-rich degradation toward increasingly resistant polysaccharide- and lignin-derived char-forming transformations.

[Insert Table 8 here]

Table 8. Conversion-dependent activation energies, E_a, obtained from FWO and Friedman isoconversional methods within the active devolatilization region, $\alpha \geq 0.4$

Conversion (α)	E_a,FWO (kJ/mol)	R^2 (FWO)	E_a,Friedman (kJ/mol)	R^2 (Friedman)
0.4	194.95	0.885	159.35	0.981
0.5	194.31	0.94	196.03	0.986
0.6	198.13	0.958	210.82	0.989
0.7	203.2	0.969	220.69	0.991
0.8	209.7	0.977	229.93	0.992
0.9	219.72	0.984	241.3	0.985

[Insert Table 9 here]

Table 9. Apparent Arrhenius pre-exponential factors estimated from Friedman-derived parameters under a pseudo-first-order assumption

Conversion (α)	lnA (s^{-1})	Apparent A (s^{-1})
0.4	32.9	1.94×10^{14}
0.5	41.91	1.59×10^{18}

0.6	45.48	5.62×10^{19}
0.7	47.76	5.51×10^{20}
0.8	49.75	4.04×10^{21}
0.9	51.94	3.61×10^{22}

3.10 Operational validation and agroindustrial application window

The conversion–temperature map was used to evaluate whether the stage-normalized conversion, α_2, could guide thermal-processing severity during chontaduro rachis valorization. Three conversion targets were selected within the active devolatilization region: α_2 = 0.50, 0.70, and 0.90, representing mild devolatilization, intermediate torrefaction-like treatment, and advanced carbon-enrichment, respectively. These treatment levels are consistent with the severity progression commonly described for torrefaction and mild carbonization, where increasing temperature or conversion promotes moisture removal, partial devolatilization, oxygenated functionality loss, and progressive carbon enrichment of the solid fraction [55, 35, 37].

As shown in **Fig. 7A**, the experimentally observed **α₂** values were close to the target conversion levels, with low prediction errors (MAE = 0.013, RMSE = 0.014, and maximum error = 0.020). This agreement indicates that the TGA-derived conversion–temperature map can serve as a practical reference for selecting treatment temperatures and controlling thermal severity. Similar approaches using TGA-derived kinetic or conversion information have been proposed for supporting biomass torrefaction, thermal conversion modeling, and solid-fuel upgrading, because thermogravimetric behavior provides useful information on degradation intervals, reactivity, and process severity [56, 57, 33].

Fig. 7B links the observed conversion levels with product-quality descriptors. As α_2 increased, the solid yield decreased from approximately 78.4% under mild treatment to 53.9% under advanced treatment, while fixed carbon increased from approximately 21.6% to 42.4%. Volatile matter decreased with conversion, and ash content increased slightly as organic matter was progressively removed. This behavior is consistent with torrefaction and carbonization mechanisms reported for lignocellulosic biomass, where increasing treatment severity reduces mass and volatile content while concentrating fixed carbon and mineral ash in the solid product [58, 35, 36].

From an application standpoint, the combined interpretation of **Fig. 7A** and **Fig. 7B** enables selection of thermal-processing windows according to the desired product. A mild α_2 target can be selected when high solid recovery is prioritized, an intermediate α_2 target can be used for torrefaction-like upgrading, and an advanced **α₂** target can be applied when a more carbon-enriched solid is desired. This trade-off between solid retention and carbon enrichment is a central consideration in biomass torrefaction, because the process improves fuel/material quality but progressively decreases mass yield as severity increases [55, 57, 37].

Therefore, the operational results complement the differential master-plot and isoconversional kinetic analyses. While the master-plot analysis identifies the best apparent kinetic descriptor for active devolatilization, the operational plots evaluate whether the conversion-based kinetic treatment can guide practical decisions related to treatment temperature, severity level, and product targeting. This distinction is important because a kinetic model becomes more useful for agroindustrial implementation when it can be linked not only to thermal-analysis fitting, but also to predictable product-property changes under controlled processing conditions [8, 33, 56].

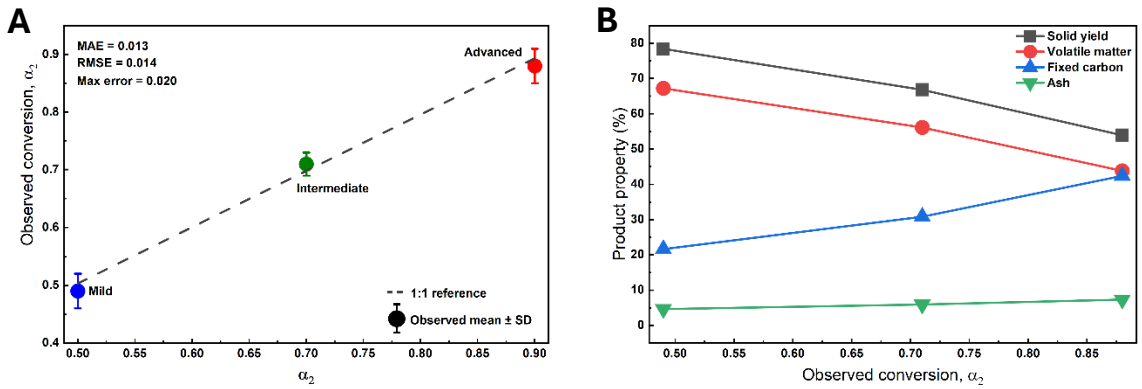


Fig 7 Operational validation of the conversion-temperature map for chontaduro rachis thermal valorization. (A) Target α_2 values predicted from the kinetic map compared with experimentally observed alpha2 after thermal treatment. (B) Evolution of solid yield, volatile matter, fixed carbon, and ash content as a function of observed α_2

4. Conclusions

This study demonstrated that chontaduro (*Bactris gasipaes* Kunth) rachis is a fiber-rich agro-industrial residue with a complex and conversion-dependent thermal decomposition behavior. The integration of proximate composition, multi-rate TGA/DTG, DSC, EGA-MS, master-plot analysis, and isoconversional kinetic modeling allowed the thermal conversion pathway of this biomatrix to be resolved beyond a simple dehydration–degradation sequence. Thermal decomposition occurred through three main regimes: an initial dehydration stage between 25 and 150 °C, an active devolatilization stage between approximately 162 and 277 °C, and a prolonged high-temperature carbonization/cracking region extending up to 700 °C. The active devolatilization region accounted for the dominant mass-loss event, with approximately 35–37% mass loss, confirming that this interval represents the critical transformation window for thermal valorization of chontaduro rachis.

The coupled EGA-MS results provided mechanistic support for the interpretation of the TGA/DTG and DSC profiles. The synchronized evolution of CO_2-related fragments, H_2O-related fragments, and NH_3-related or nitrogen-containing signals near the principal DTG maximum indicated that the main devolatilization stage involved overlapping decarboxylation, dehydration, and deamination reactions. These volatile signatures were consistent with the degradation of carbohydrate-rich domains, residual proteinaceous constituents, and oxygenated structural groups within the lignocellulosic matrix. At higher temperatures, delayed ion-current maxima associated with hydrocarbon, oxygenated, and nitrogen-containing fragments supported the occurrence of secondary cracking, aromatization, and progressive reorganization of the residual carbonaceous matrix.

The kinetic analysis confirmed that the thermal decomposition of chontaduro rachis cannot be adequately described by a single global reaction. Although the Kissinger method provided a useful global apparent activation energy of 182.05 kJ mol^{-1}, the Flynn–Wall–Ozawa and Friedman methods revealed conversion-dependent activation barriers. The FWO activation energy increased from 194.95 to 219.72 kJ mol^{-1}, while Friedman values increased from 159.35 to 241.30 kJ mol^{-1} within the selected active devolatilization interval. This progressive increase in activation energy indicates a transition from the decomposition of more labile amorphous carbohydrate-rich structures toward increasingly resistant cellulose- and lignin-derived domains.

The master-plot and thermal-shift analyses further supported the multi-step nature of the active devolatilization process. The differential master plot identified an Avrami–Erofeev-type A3 function as the best apparent descriptor of the normalized devolatilization-rate profile; however, this model should be interpreted as a macroscopic kinetic descriptor rather than as proof of a unique microscopic mechanism. In addition, the conversion-dependent thermal-shift factors showed that heating-rate effects were not uniform across the active devolatilization stage. Instead, the temperature shifts depended on conversion level, indicating the combined influence of pseudo-component overlap, thermal lag, volatile diffusion, and progressive char-forming reactions.

From an applied perspective, the conversion–temperature map provided a practical framework for selecting thermal-processing windows for chontaduro rachis valorization. The mild treatment condition near $\alpha_2 = 0.50$ favored higher solid recovery, the intermediate condition near $\alpha_2 = 0.70$ represented a torrefaction-like upgrading window, and the advanced condition near $\alpha_2 = 0.90$ promoted stronger carbon enrichment. The operational assessment showed that increasing α_2 reduced solid yield from approximately 78.4% to 53.9%, while fixed carbon increased from approximately 21.6% to 42.4%, demonstrating a clear trade-off between solid retention and carbon enrichment. These results indicate that the α_2-based kinetic map can support temperature selection, treatment-severity control, and product targeting for agroindustrial thermal processing.

Declarations

Funding

The authors did not receive support from any organization for the submitted work.

Competing interests

The authors declare that they have no competing interests.

Ethics approval

Not applicable. This study did not involve human participants, human data, human tissue, or animals.

Consent to participate

Not applicable.

Consent for publication

Not applicable.

Data availability

The datasets generated and analyzed during the current study are provided as Online Resources 1–3. Online Resource 1 contains the raw TGA/DTG, DSC, and EGA-MS datasets. Online Resource 2 contains the master-plot, thermal-shift, Kissinger, Flynn–Wall–Ozawa, Friedman, and activation-thermodynamic datasets. Online Resource 3 contains the operational validation dataset, product-property descriptors, and prediction-error metrics. Additional data are available from the corresponding author upon reasonable request.

Author contributions

Oscar Danilo Guerra Ceballos: conceptualization, methodology, investigation, formal analysis, data curation, visualization, and writing—original draft. Wilson Daniel Caicedo Chacon: conceptualization, supervision, validation, writing—review and editing, project administration, and correspondence. Both authors read and approved the final manuscript.

Acknowledgments

The authors gratefully acknowledge the Universidad Autónoma de Occidente for supporting the thermal characterization analyses carried out in this study. Special thanks are extended to Professor Gladis Miriam Aparicio Rojas for her valuable assistance, technical support, and institutional collaboration during the thermoanalytical characterization of the chontaduro rachis biomass.

References

1. Šelo G, Planinić M, Tišma M, Tomas S, Koceva Komlenić D, Bucić-Kojić A (2021) A comprehensive review on valorization of agro-food industrial residues by solid-state fermentation. Foods 10:927. https://doi.org/10.3390/foods10050927

2. Spacki KC, Corrêa RCG, Uber TM, Barros L, Ferreira ICFR, Peralta RA, Moreira RFM, Helm CV, Lima EA, Bracht A, Peralta RM (2022) Full exploitation of peach palm (Bactris gasipaes Kunth): state of the art and perspectives. Plants 11:3175. https://doi.org/10.3390/plants11223175

3. Mujtaba M, Fraceto LF, Fazeli M, Mukherjee S, Savassa SM, Medeiros GA, Pereira AES, Mancini SD, Lipponen J, Vilaplana F (2023) Lignocellulosic biomass from agricultural waste to the circular economy: a review with focus on biofuels, biocomposites and bioplastics. J Clean Prod 402:136815. https://doi.org/10.1016/j.jclepro.2023.136815

4. Sharma K, Konsue N, Sai-Ut S, Onsaard E, Zhang W, Wu S, Huang JQ, Jung YH, Rawdkuen S (2026) Peach palm (Bactris gasipaes) as a sustainable source of plant proteins, dietary fiber and other functional ingredients: recovery techniques and functional food applications. Foods 15:736. https://doi.org/10.3390/foods15040736

5. Vieira E, Nunes C, Coimbra MA et al (2021) Valorization of peach palm (Bactris gasipaes Kunth) waste: production of xylooligosaccharides from xylans. Waste Biomass Valorization. https://doi.org/10.1007/s12649-021-01457-3

6. Varol EA, Mutlu Ü (2023) TGA-FTIR analysis of biomass samples based on the thermal decomposition behavior of hemicellulose, cellulose, and lignin. Energies 16:3674. https://doi.org/10.3390/en16093674

7. Pielsticker S, Gövert B, Umeki K, Kneer R (2021) Flash pyrolysis kinetics of extracted lignocellulosic biomass components. Front Energy Res 9:737011. https://doi.org/10.3389/fenrg.2021.737011

8. Branca C, Galgano A (2024) Kinetic modelling of biomass pyrolysis processes. Processes 12:706. https://doi.org/10.3390/pr12040706

9. Risoluti R, Gullifa G, Barone L, Papa E, Materazzi S (2022) On-line thermally induced evolved gas analysis: an update—Part 1: EGA-MS. Molecules 27:3518. https://doi.org/10.3390/molecules27113518

10. Radojević M, Janković B, Stojiljković D, Jovanović V, Čeković I, Manić N (2021) Improved TGA-MS measurements for evolved gas analysis during pyrolysis process of various biomass feedstocks: syngas energy balance determination. Thermochim Acta 699:178912. https://doi.org/10.1016/j.tca.2021.178912

11. Gullifa G, Papa E, Putzolu G, Rizzo G, Ruocco M, Albertini C, Risoluti R, Materazzi S (2025) MS and GC-MS analytical methods for on-line thermally induced evolved gas analysis. Chemosensors 13:258. https://doi.org/10.3390/chemosensors13070258

12. Kissinger HE (1956) Variation of peak temperature with heating rate in differential thermal analysis. J Res Natl Bur Stand 57:217-221

13. Flynn JH, Wall LA (1966) General treatment of the thermogravimetry of polymers. J Res Natl Bur Stand A Phys Chem 70A:487-523

14. Friedman HL (1964) Kinetics of thermal degradation of char-forming plastics from thermogravimetry. Application to a phenolic plastic. J Polym Sci C Polym Symp 6:183-195. https://doi.org/10.1002/polc.5070060121

15. Vyazovkin S (2020) Kissinger method in kinetics of materials: things to beware and be aware of. Molecules 25:2813. https://doi.org/10.3390/molecules25122813

16. Koga N, Vyazovkin S, Burnham AK, Favergeon L, Muravyev NV, Pérez-Maqueda LA, Saggese C, Sánchez-Jiménez PE (2022) ICTAC Kinetics Committee recommendations for analysis of thermal decomposition kinetics. Thermochim Acta 719:179384. https://doi.org/10.1016/j.tca.2022.179384

17. Hames B, Ruiz R, Scarlata C, Sluiter A, Sluiter J, Templeton D (2008) Preparation of samples for compositional analysis. Laboratory Analytical Procedure NREL/TP-510-42620. National Renewable Energy Laboratory, Golden

18. ASTM International (2024) ASTM E1757-19: Standard practice for preparation of biomass for compositional analysis. ASTM International, West Conshohocken

19. Tian Y, Perré P (2023) Effects of particle size on the pyrolysis of spruce and poplar: thermogravimetric analyses, DAEM modelling, validation, and prediction of secondary charring. Biomass Bioenergy 176:106913. https://doi.org/10.1016/j.biombioe.2023.106913

20. Han FY, Wang M, Ma XB, Chen DZ, Liu ZQ, Zhang RN (2023) Numerical simulation of heat transfer properties of large-sized biomass particles during pyrolysis process. Heliyon 9:e21255. https://doi.org/10.1016/j.heliyon.2023.e21255

21. Paredes R, Castells B, Tascón A (2024) Thermogravimetric assessment of biomass: unravelling kinetic, chemical composition and combustion profiles. Fire 7:396. https://doi.org/10.3390/fire7110396

22. AOAC International (2023) Official Methods of Analysis of AOAC International, 22nd edn. AOAC International, Rockville

23. McCleary BV (2023) Measurement of dietary fiber: which AOAC Official Method of AnalysisSM to use. J AOAC Int 106:917-930. https://doi.org/10.1093/jaoacint/qsad051

24. Velázquez Martí B, Gaibor-Chavez J, López Cortés I, Olivares Aguilar LE (2023) Evaluation of the intermediate values of the TGA curves as indicators of the proximal analysis of biomass. Agronomy 13:2552. https://doi.org/10.3390/agronomy13102552

25. Emiola-Sadiq T, Zhang L, Dalai AK (2021) Thermal and kinetic studies on biomass degradation via thermogravimetric analysis: a combination of model-fitting and model-free approach. ACS Omega 6:22233-22247. https://doi.org/10.1021/acsomega.1c02937

26. Bondarchuk I, Bondarchuk S, Vorozhtsov A, Zhukov A (2023) Advanced fitting method for the kinetic analysis of thermogravimetric data. Molecules 28:424. https://doi.org/10.3390/molecules28010424

27. Sánchez-Jiménez PE, Pérez-Maqueda LA, Perejón A, Criado JM (2013) Generalized master plots as a straightforward approach for determining the kinetic model: the case of cellulose pyrolysis. Thermochim Acta 552:54-59. https://doi.org/10.1016/j.tca.2012.11.003

28. Criado JM, Pérez-Maqueda LA, Ortega A (1994) Development of master curves for discriminating the mechanism of solid state reactions from experimental data obtained by using the cyclic and controlled rate thermal analysis. J Therm Anal 41:1535-1541. https://doi.org/10.1007/BF02549951

29. Khawam A, Flanagan DR (2006) Solid-state kinetic models: basics and mathematical fundamentals. J Phys Chem B 110:17315-17328. https://doi.org/10.1021/jp062746a

30. Ozawa T (1965) A new method of analyzing thermogravimetric data. Bull Chem Soc Jpn 38:1881-1886. https://doi.org/10.1246/bcsj.38.1881

31. Mianowski A, Szul M (2025) Practical aspects of the analysis of thermal dissociation and pyrolysis processes in terms of transition state theory. Energies 18:2619. https://doi.org/10.3390/en18102619

32. El-Sayed SA, Khass TM, Mostafa ME (2023) Thermal degradation behaviour and chemical kinetic characteristics of biomass pyrolysis using TG/DTG/DTA techniques. Biomass Convers Biorefin. https://doi.org/10.1007/s13399-023-03926-2

33. Teh JS, Teoh YH, How HG, Sher F (2021) Thermal analysis technologies for biomass feedstocks: a state-of-the-art review. Processes 9:1610. https://doi.org/10.3390/pr9091610

34. Janković B, Manić N, Stojiljković D (2019) The gaseous products characterization of the pyrolysis process of various agricultural residues using TGA-DSC-MS techniques. J Therm Anal Calorim 139:3091-3106. https://doi.org/10.1007/s10973-019-08733-4

35. Zheng Y, Tao L, Yang X, Huang Y, Liu C, Gu J, Zheng Z (2017) Effect of the torrefaction temperature on the structural properties and pyrolysis behavior of biomass. BioResources 12:3425-3447

36. Liu P, Lang P, Lu A, Li Y, Li X, Sun T, Yang Y, Li H, Lei T (2022) Effect of evolution of carbon structure during torrefaction in woody biomass on thermal degradation. Int J Environ Res Public Health 19:16831. https://doi.org/10.3390/ijerph192416831

37. Nair SC, John V, Bai RG, Kikas T (2025) Torrefaction of lignocellulosic biomass: a pathway to renewable energy, circular economy, and sustainable agriculture. Sustainability 17:7738. https://doi.org/10.3390/su17177738

38. Escalante J, Chen WH, Tabatabaei M, Hoang AT, Kwon EE, Lin KYA, Saravanakumar A (2022) Pyrolysis of lignocellulosic, algal, plastic, and other biomass wastes for biofuel production and circular bioeconomy: a review of thermogravimetric analysis (TGA) approach. Renew Sustain Energy Rev 169:112914. https://doi.org/10.1016/j.rser.2022.112914

39. Kaczor Z, Buliński Z, Werle S (2020) Modelling approaches to waste biomass pyrolysis: a review. Renew Energy 159:427-443. https://doi.org/10.1016/j.renene.2020.05.110

40. Tao W, Gao L, Li M, Wang Y, Shi L, Xu C, Lu X, Pan B (2026) Effect of initial water content on the pyrolysis mechanism of lignocellulosic biomass. Biochar. https://doi.org/10.1007/s42773-026-00629-5

41. Hu B, Xie W, Li H, Li K, Lu Q, Yang Y et al (2020) On the mechanism of xylan pyrolysis by combined experimental and computational approaches. Proc Combust Inst 38:4215-4223. https://doi.org/10.1016/j.proci.2020.06.172

42. Lu X, Gu X (2022) A review on lignin pyrolysis: pyrolytic behavior, mechanism, and relevant upgrading for improving process efficiency. Biotechnol Biofuels Bioprod 15:106. https://doi.org/10.1186/s13068-022-02203-0

43. Bielecki M, Zubkova V (2023) Analysis of interactions occurring during the pyrolysis of lignocellulosic biomass. Molecules 28:506. https://doi.org/10.3390/molecules28020506

44. Wang W, Lemaire R, Bensakhria A, Luart D (2022) Thermogravimetric analysis and kinetic modeling of the AAEM-catalyzed pyrolysis of woody biomass. Molecules 27:7662. https://doi.org/10.3390/molecules27227662

45. Wang W, Lemaire R, Bensakhria A, Luart D (2022) Analysis of the catalytic effects induced by alkali and alkaline earth metals (AAEMs) on the pyrolysis of beech wood and corncob. Catalysts 12:1505. https://doi.org/10.3390/catal12121505

46. Ionita D, Cristea M, Cosmulescu SF, Predeanu G, Harabagiu V, Samoila P (2023) Thermal and viscoelastic responses of selected lignocellulosic wastes: similarities and differences. Polymers 15:2100. https://doi.org/10.3390/polym15092100

47. Chen Q, Yang R, Zhao B, Li Y, Wang S, Wu H, Zhuo Y, Chen C (2014) Investigation of heat of biomass pyrolysis and secondary reactions by simultaneous thermogravimetry and differential scanning calorimetry. Fuel 134:467-476. https://doi.org/10.1016/j.fuel.2014.05.092

48. Ming X, Xu F, Jiang Y, Zong P, Wang B, Li J et al (2019) Thermal degradation of food waste by TG-FTIR and Py-GC/MS: pyrolysis behaviors, products, kinetic and thermodynamic analysis. J Clean Prod. https://doi.org/10.1016/j.jclepro.2019.118713

49. Mehrabian R, Scharler R, Obernberger I (2012) Effects of pyrolysis conditions on the heating rate in biomass particles and applicability of TGA kinetic parameters in particle thermal conversion modelling. Fuel 93:567-575. https://doi.org/10.1016/j.fuel.2011.09.054

50. Dorez G, Ferry L, Sonnier R, Taguet A, Lopez-Cuesta JM (2014) Effect of cellulose, hemicellulose and lignin contents on pyrolysis and combustion of natural fibers. J Anal Appl Pyrolysis 107:323-331. https://doi.org/10.1016/j.jaap.2014.03.017

51. Silva J, Teixeira S, Teixeira J (2023) A review of biomass thermal analysis, kinetics and product distribution for combustion modeling: from the micro to macro perspective. Energies 16:6705. https://doi.org/10.3390/en16186705

52. Cai J, He Y, Yu X, Banks SW, Yang Y, Zhang X, Yu Y, Liu R, Bridgwater AV (2017) Review of physicochemical properties and analytical characterization of lignocellulosic biomass. Renew Sustain Energy Rev 76:309-322. https://doi.org/10.1016/j.rser.2017.03.072

53. Wang S, Dai G, Yang H, Luo Z (2017) Lignocellulosic biomass pyrolysis mechanism: a state-of-the-art review. Prog Energy Combust Sci 62:33-86. https://doi.org/10.1016/j.pecs.2017.05.004

54. Kristanto J, Azis MM, Purwono S (2021) Multi-distribution activation energy model on slow pyrolysis of cellulose and lignin in TGA/DSC. Heliyon 7:e07669. https://doi.org/10.1016/j.heliyon.2021.e07669

55. Tumuluru JS, Sokhansanj S, Hess JR, Wright CT, Boardman RD (2011) A review on biomass torrefaction process and product properties for energy applications. Ind Biotechnol 7:384-401. https://doi.org/10.1089/ind.2011.0014

56. Lee CG, Kim MJ, Eom CD (2022) Kinetic study of torrefied woody biomass via TGA using a single heating rate and the model-fitting method. BioResources 17:411-428

57. Ivanovski M, Petrovic A, Ban I, Goricanec D, Urbancl D (2021) Determination of the kinetics and thermodynamic parameters of lignocellulosic biomass subjected to the torrefaction process. Materials 14:7877. https://doi.org/10.3390/ma14247877

58. Urbancl D, Agačević D, Gradišnik E, Šket A, Štajnfelzer N, Goričanec D, Petrovič A (2025) The torrefaction of agricultural and industrial residues: thermogravimetric analysis, characterization of the products and TG-FTIR analysis of the gas phase. Energies 18:4648. https://doi.org/10.3390/en18174648

Supplementary Files

This is a list of supplementary files associated with this preprint. Click to download.

- SupplementaryMaterialS1RawTGADSCEGAMSData.xlsx
- SupplementaryMaterialS2MasterPlotsKineticAnalysis.xlsx
- SupplementaryMaterialS3OperationalValidationData.xlsx